RSC Advances

PAPER

View Article Online
View Journal | View Issue

Cite this: *RSC Adv.*, 2025, **15**, 22587

Integrated SA-CMC hydrogel formulation with the NAA hormone, ZnO nanoparticles, and potassium chloride: a sustainable approach to enhance flowering and crop yield in the short-term crop chili (*Capsicum annuum*)†

Loshini Rodrigo, [a] Imalka Munaweera *[a] and Pamoda Thavish Perera[b]

Rising food demand due to population growth and the low nutrient use efficiency (NUE) of conventional fertilizers necessitate environmentally friendly, effective agrochemical delivery systems. Hydrogels are innovative materials, and an integrated hydrogel formulation encapsulated with zinc oxide nanoparticles (ZnO NPs), potassium chloride and naphthalene acetic acid (NAA) was synthesized in this study to increase the flowering and crop yield of the short-term crop chili. ZnO NPs were synthesized *via* the co-precipitation method and characterized *via* XRD, SEM and FTIR techniques. The synthesized hydrogels were characterized using SEM and FTIR techniques. The swelling capacity of the hydrogels peaked at 202.04% on day 14, and they exhibited biodegradation by day 20, with a weight loss of 99.98%. Biodegradation findings were corroborated by optical microscopy pictures. Atomic absorption spectrometry was used to study the release of potassium and zinc nutrients from the hydrogels on days 1, 7, 14, and 21, suggesting the slow-release behavior of the hydrogels. UV-VIS spectrophotometry was used to study the NAA hormone, which revealed a higher encapsulation efficiency of 92.53% with a sustained, slow-release profile over a 21-day period. The exponential phase of the NAA-release profile matched well with the Higuchi model (R^2 = 0.97). The parameters plant height, number of branches, flowers, pods and yield at first plucking were statistically analyzed using the analysis of variance (ANOVA), and significant differences between each sample were analyzed using Tukey pairwise comparison at a significance level of 0.05. Significant enhancements observed in flowering and yield were attributed to the synergistic effect of the encapsulated agrochemicals in the hydrogels. The ability to biodegrade and improve NUE positions this integrated hydrogel formulation as a sustainable alternative for modern agriculture.

Received 17th May 2025
Accepted 19th June 2025

DOI: 10.1039/d5ra03488d

rsc.li/rsc-advances

1. Introduction

Global population has been steadily increasing and is projected to surpass 9.6 billion by 2050, necessitating an increase in food production to cater to its needs, which will consequently worsen food-shortage issues.[1,2] Water scarcity, degradation of soil quality, loss of biodiversity, and an increased level of greenhouse gas emissions pose significant threats to existing agricultural practices as they are unfavorable to our planet and its future.[3,4] Additionally, climate change over the past decades has intensified the depletion of various natural resources, leading to desertification and thereby reducing agricultural productivity and overall crop yield.[5,6] Therefore, the challenges of producing adequate agricultural products while conserving the environment lie ahead of the world. Natural sources of water and soil are often overused in fulfilling the agricultural needs of this ever-growing population owing to the excessive use of fertilizers and pesticides.[8] The lower nutrient use efficiency (NUE) of conventional fertilizers is a major reason for this consequence, and as reported by Govil *et al.*, only 30–35% of the applied nutrients are absorbed by crops.[9] Reportedly, 50–70% of the nitrogen fertilizers applied are lost owing to volatilization, denitrification and leaching, causing contamination of groundwater and degrading soil quality.[10,11] Furthermore, nutrient deficiencies and hormone imbalances trigger flower and fruit drop, constraining sufficient crop yield and productivity. Innovative solutions to improve the efficiency of agrochemical usage while achieving sustainable food security are of paramount importance in the current agricultural context.

[a]*Department of Chemistry, University of Sri Jayewardenepura, Nugegoda, 10250, Sri Lanka. E-mail: imalka@sjp.ac.lk*

[b]*Research and development division, Panam Biotech Pvt (Ltd), Homagama, 10200, Sri Lanka*

† Electronic supplementary information (ESI) available. See DOI: https://doi.org/10.1039/d5ra03488d

Capsicum annuum (chili) is an important vegetable crop due to its economic and nutritional value. It is a short-term crop that demands rapid and efficient nutrient uptake to support its high flowering and fruiting rates, which are critical for maximizing yield within a limited growing period. The crop requires optimal temperatures (around 20–25 °C) and is sensitive to environmental stresses, which can cause flowers and young fruit to drop, reducing yield. Additionally, high flowering demand necessitates sufficient nutrient availability to support fruit set and development; however, rapid nutrient depletion can lead to deficiencies impacting fruit size and quality.[7] As inadequate nutrient management stands as a barrier to harvesting a higher yield in chili, opting for innovative nutrient delivery systems that can provide sustained, targeted nutrient release aligned with the rapid and high nutrient demands of crops is imperative.[12] This highlights the importance of studying advanced formulations, which can potentially enhance nutrient use efficiency, regulate hormone-mediated growth responses, and improve productivity in *Capsicum annuum*, the focus of this study. The synthesized formulation in this study aimed to overcome nutrient loss and cater to high flowering demand by slow and sustained nutrient release and hormonal regulation, ultimately improving plant productivity and crop yield in short-term cropping systems.

Slow-release fertilizers are positioned as a potential alternative to address the unfavorable properties of conventional fertilizers.[13] Fertilizers that delay the availability of nutrients for plant uptake and use after application are defined as slow-release fertilizers by the Association of American Plant Food Control Officials (AAPFCO).[14] Hydrogels are positioned as a game-changing material that has the potential to mitigate existing obstacles in conventional fertilizers and ensure sustainability as they contribute to the slow release of encapsulated active ingredients within the polymer matrix.[15] Hydrogels are soft, water-swollen, cross-linked, three-dimensional macromolecular networks of hydrophilic copolymers that can incorporate large amounts of water or agrochemicals into their structure and release them depending on the surrounding conditions and requirements of plants.[16–18] Hydrogels, which have the ability to absorb water several hundred times their dry weight, are named as superabsorbent hydrogels (SAHs) on account of their hydrophilic groups, which do not allow dissolution in water due to the grafted polymeric network.[19] Furthermore, the combination of SAHs with fertilizers produces slow-release fertilizer hydrogels with the advantage of regulating nutrients and water in one material as they absorb and release them slowly for an extended period of time, a characteristic in contrast to the conventional fertilizers. Additionally, they positively affect plant nutrition, reduce evaporation losses and the frequency of irrigation, while functioning as "mini reservoirs" supplying water and fertilizers to plants influenced by osmotic pressure differences.[20–23] While hydrogels are synthesized using both natural and synthetic polymers, natural polymers, such as starch, alginate, cellulose, chitosan, and lignin, have gained considerable interest due to the benefits of biodegradability, low cost and abundance.[24,25] Sodium alginate (SA) and carboxymethyl cellulose (CMC), which are hydrophilic and biodegradable polymers, were used in this research study to formulate the hydrogel matrix. SA is a natural polysaccharide composed of β-D-mannose uronic acid (M blocks) and α-L-guluronic acid (G Blocks) derived from brown algae with good biocompatibility and degradability. SA has many hydrophilic carboxyl and hydroxyl groups, which facilitate better cross-linking, modification, and grafting, while CMC is a cellulose derivative that is soluble in aqueous media due to the $-CH_2-$COOH groups attached to some of the –OH groups in cellulose units.[26,27] Ionic cross-linking, a method of physical crosslinking, is used in this study, in which $CaCl_2$ is used to cross-link, as the divalent cation Ca^{2+}, upon addition to the hydrogel precursor, induces gel formation owing to the abundant anionic groups present in SA and CMC.[28,29] The gelling properties, which enable the formation of gels and the almost temperature-independent sol–gel transition in the presence of multivalent cations like Ca^{2+}, make alginate an ideal candidate for preparing biomaterials with slow-release mechanisms.[30–33] Gel formation is driven by interactions between G blocks, which participate in forming tightly held junctions, in the presence of Ca^{2+} ions that act as cross-links between the functional groups of alginates.[34] Here, an incident of "zipping" occurs in which a G block in one polymer forms junctions with a G block of an adjacent polymer through interactions with the carboxylic groups in the sugars, resulting in the gel network. This metal-chelation binding chain is called the "egg-box" model of cross-linking on account of the structural form of the G block.[34] While the possibility of synthesizing the hydrogels using natural or/and synthetic polymers exists, utilizing synthetic polymers to formulate hydrogels is less-environmentally friendly as they undergo degradation upon exposure to external environmental factors resulting microparticles and toxic by-products, causing neurotoxic and carcinogenic problems, in addition to possible contamination of soil and food.[35] The half-life of synthetic hydrogels is found to be 5–7 years, which is the time taken to degrade into carbon dioxide, ammonium and water, paving the way for environmental pollution.[19] The biodegradability of natural polymers was the focus of this study, and thus, SA and CMC were used to synthesize the polymer matrix. The slow-release urea fertilizer synthesized based on sodium alginate/carboxymethyl chitosan hydrogels by Arafa *et al.* exhibited biodegradation in soil in addition to the slow release of urea.[36] Similarly, El Idrissi *et al.* demonstrated a urea-rich SA hydrogel with excellent water retention and sustained nitrogen release over nine weeks, confirming its biodegradability and positive effects on plant growth under water-deficit conditions.[26] Natural degradation rather than bioaccumulation in soil has attracted considerable interest in biopolymer-based hydrogels, supporting the global need to opt for eco-friendly and sustainable approaches to using agrochemicals while improving nutrient use efficiency.

Agriculture is advancing, with nanotechnology serving as a pioneering technology that fosters sustainability. In this research, nanotechnology was integrated, and Fig. 1 illustrates the research design. Nanotechnology was incorporated into this work by utilizing nanofertilizers that contained the micronutrient zinc (Zn) in the form of zinc oxide nanoparticles (ZnO

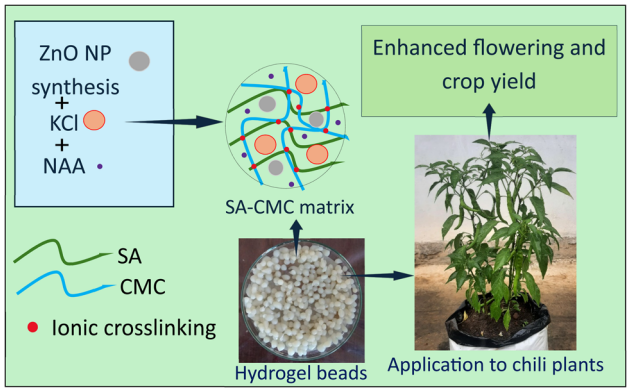

Fig. 1 Research design.

NPs). Nanoparticles are found to provide the best boost for improved plant nutrition as they are within the nanorange (1–100 nm), which increases the points of interaction due to the high area-to-volume ratio. This, in turn, amplifies the contact points for the fertilizer uptake by plants.[37,38] Zn is responsible for regulating enzyme functioning in plants, as well as protein synthesis, which promotes growth and biomass yield in the long run.[34,39,40] ZnO NPs are known for their stress-tolerant abilities as well as significant anti-microbial properties.[34,41] Nanoparticles' ability to penetrate, uptake and translocate has proven to provide plants with nutrition in a steady manner, providing a solution to an inherent shortcoming of conventional fertilizers.[42]

Furthermore, the use of ZnO NPs has been shown to be more cost-effective and efficient than bulk ZnO, thereby improving plant productivity by enabling lower fertilizer doses, enhancing nutrient uptake and yield, and supporting sustainable agriculture. Dimkpa *et al.* reported that coating urea with low-dose ZnO NPs increased wheat grain yield by 39–51% under drought conditions, whereas bulk ZnO showed insignificant yield gains despite higher Zn application rates. This demonstrates that ZnO NPs enhance nutrient uptake and plant performance more efficiently than bulk ZnO.[43] Although ZnO NPs per kilogram are more expensive, their higher efficacy at lower doses can result in better economic efficiency by increasing crop yield and reducing the amount of Zn applied. Large-scale production and optimized application rates can further improve their cost-effectiveness.[44] Additionally, the economic feasibility of producing ZnO nanoparticles *via* green synthesis has been confirmed, with profitable investment returns achievable in approximately three years, supporting their scalable and cost-effective production.[45]

Additionally, notable advantages of encapsulation of ZnO NPs in hydrogel formulations have been reported in the literature. Soto-Gonzales *et al.* reported that the integration of ZnO NPs into hydrogels significantly enhanced Quinoa seed germination and plant establishment compared to controls.[46] Uysal *et al.* carried out research on wheat in which ZnO NPs were synthesized using rosemary extract, then integrated into a cross-linked polymer matrix, which promoted root and shoot elongation more effectively than suspended NPs, proving the efficacy of using nanoparticle-hydrogel composites in plant breeding and demonstrating their potential in future agricultural applications.[47] Radmehr *et al.* designed a novel antimicrobial superabsorbent hydrogel *via* the copolymerization of CMC and acrylic acid (AAc) by incorporating ZnO NPs through gamma radiation, which exhibited better swelling capacity, thermal stability, and antibacterial activity against *Escherichia coli*, making it a promising and novel candidate for biomedical and environmental applications.[48] It is also found that incorporating metal oxide nanoparticles into the hydrogel matrix improved its swelling capacity and mechanical strength.[25]

Potassium (K) is an essential macronutrient that plays a vital role in physiological processes, such as photosynthesis, enzyme activation, osmoregulation, and reproductive development, which in turn affect flowering, fruit set, and overall yield quality in short-term crops like chili. Based on this, potassium chloride (KCl) was encapsulated in the hydrogel formulation in this study. Studies have shown that an optimal amount of K significantly enhances chili seedling growth, leaf development, and fruit yield, while K deficiency can lead to reduced fruit size and lower capsaicin content in chili, making plants more prone to environmental stresses.[42–51] Chen *et al.* reported that encapsulating KCl in starch-alginate matrix cross-linked with $CaCl_2$ exhibited controlled release of K while higher SA concentrations resulted in more uniform beads, reduced swelling, and slower K release rates.[52]

Plant growth regulators (PGRs) are naturally occurring or synthetic compounds that regulate plant growth and development by modulating metabolic and physiological processes. They help plants tolerate abiotic stresses by altering plant physiology and morphology, improving growth, yield, and stress resilience.[53] PGRs are Active Substances (AS) of "Plant Protection Products" (PPP), as categorized by European Union (EU) with specific mode of action, which are used to modify plant growth such as increasing branching, suppressing shoot growth, increasing frequency of flowering, removing excess fruit, or altering fruit maturity.[53] Naphthalene acetic acid (NAA) hormone, which was used in this study, is considered as an active substance categorized under PPP in EU.[53] NAA is a synthetic auxin hormone, a PGR that plays an important role in promoting cell division and expansion, inducing the formation of adventitious roots, increasing fruit setting, and preventing fruit drop.[54] Apart from hastening fruit maturity and producing better-quality fruits, NAA increases the number of branches, fresh weight and fruit yield. Singh *et al.* reported that the application of 100 ppm of NAA on tomato yielded the highest number of branches and fruits per plant and fruit weight, compared to the other controls.[55] Khan *et al.* reported that ZnO NPs combined with PGRs can mitigate various abiotic stresses, such as drought, salinity, and temperature extremes, by improving plant growth at morphological, physiological, biochemical, and ultrastructural levels.[56] Khardia *et al.* conducted research on the effect of PGRs and Zn fertilization on the growth of pearl millet and reported that the interaction effect of PGRs (triacontanol and NAA) and Zn fertilization exhibited a significant effect on plant height and dry matter

accumulation, indicating that PGRs combined with Zn enhance growth and developmental processes, contributing to improved plant vigor and stress tolerance, acting as a plant protection product.[57] Furthermore, the study carried out by Jan *et al.* concluded that drought tolerance in sunflower was significantly increased by increasing relative water content (RWC), free proline, total phenolic compounds, and antioxidant enzyme activities upon foliar application of Zn (as $ZnSO_4$), K (as KNO_3) and gibberellic acid (GA3).[58]

These studies demonstrate that combining PGRs with Zn and K can serve as effective plant protection products rather than just traditional fertilizers, as their synergistic effect enhances plant physiological performance, stress tolerance, and nutrient uptake, which contribute to improved growth, yield, and quality.

To the best of our knowledge, the encapsulation of NAA hormone alongside ZnO NPs and KCl in a biodegradable SA-CMC hydrogel formulation for chili has not been studied previously, endorsing the novelty of this study.

The SA-CMC-based hydrogel formulation encapsulated with NAA hormone, ZnO NPs, and KCl could be positioned as an innovative "plant production product" rather than a conventional fertilizer, as it integrates multiple functionalities beyond nutrient supply. Unlike traditional fertilizers that primarily provide nutrients, this hydrogel system offers a slow and sustained release of nutrients, plant hormonal regulation, water retention and soil conditioning, as well as ZnO NPs-enabled micronutrient delivery, biodegradability and enhanced flowering and crop yield in chili. Therefore, this study presents a novel approach to synchronize nutrient-hormone delivery through the synthesis of SA-CMC-based, integrated hydrogel formulation for enhanced flowering and crop yield in chili as a sustainable agricultural practice.

2. Experimental

2.1 Chemicals, materials and instruments

SA, CMC, KCl, and NAA, were purchased from Glorchem (Pvt.) Ltd. $CaCl_2$, sodium hydroxide pellets, PVA, zinc acetate, acetone, HCl, and HNO_3 were purchased from Sigma-Aldrich. All the chemicals used in this research were of analytical grade and used without further purification. In all experiments, distilled water was used.

The crystalline structure of synthesized nanoparticles was analyzed by powder X-ray diffraction (XRD) patterns recorded using a X-ray Powder Diffractometer of Rigaku smart lab, 3 kW sealed X-ray tube in the range of 20–80, two theta degree range at a rate of 6/minute. The morphology of nanoparticles and hydrogel beads was analyzed using scanning electron microscopy (SEM) imaging with a ZEISS model, operating in a secondary electron mode, at an accelerating voltage of 10 kV. Functional groups and relevant peak positions were studied using a PerkinElmer Inc. Spectrum Two Fourier transform infrared (FTIR) spectrometer in the range from 4000 to 400 cm^{-1} using the KBr pellet technique. Atomic absorption spectrometric (AAS) data were acquired sing an atomic absorption spectrometer of Thermo Scientific iCE 3000 series to analyze the chemical compositions of metals in the synthesized hydrogels. The UV-VIS spectrometry data for the quantification of NAA hormone were obtained using a double-beam UV-VIS spectrometer from PerkinElmer, LAMBDA 365+ at $\lambda = 222$ nm. Microscopy images of the hydrogel beads to study their degradability were obtained from an Olympus CX23 optical microscope at 40× magnification. Image J software was used to plot size distribution graphs.

2.2 Methodology

2.2.1. Synthesis of zinc oxide nanoparticles. As the precursor, zinc acetate dihydrate ($Zn(CH_3COO)_2 \cdot 2H_2O$) was used and a surfactant-assisted method was employed. Firstly, 1 M aqueous solution of ($Zn(CH_3COO)_2 \cdot 2H_2O$) was prepared, followed by the preparation of a 2 M NaOH solution. From the prepared 0.01% PVA solution, 2 mL was added to the precursor solution and stirred magnetically until the solution was homogenous. Afterwards, the NaOH solution was added dropwise to the zinc acetate dihydrate/PVA solution for 2 hours at room temperature with continuous stirring. The white precipitate was centrifuged at 4000 rpm for 7 minutes, and the supernatant was removed and washed three times with distilled water. The obtained product was oven-dried at 100 °C for 12 hours. The dried powder was crushed using a mortar and pestle and was subsequently subjected to calcination at 650 °C for 2 hours, obtaining a fine powder of ZnO nanoparticles.[59]

2.2.2 Characterization of synthesized zinc oxide nanoparticles. Characterization of the synthesized NPs was performed using PXRD, FTIR and SEM analyses.

2.2.3 Synthesis of SA-CMC-based hydrogel beads loaded with NAA, ZnO NPs and KCl. A solution of 100 ppm NAA was prepared by dissolving 10.0 mg in 1 mL of acetone and adjusting the final volume to 25 mL with distilled water.[55] A solution of KCl was prepared by dissolving 16.67 g of KCl in 25 mL of distilled water. To synthesize the hydrogel bead, 5.00 g of SA was dissolved in 25 mL of distilled water and stirred for up to 2 hours to obtain a homogenous solution, followed by the addition of the prepared KCl solution. Afterwards, 1.00 g of CMC was dissolved in 25 mL of distilled water and heated to 50 °C, continuously stirred for 2 hours to obtain a homogeneous solution, and subsequently, 500.0 mg of the synthesized ZnO NPs and the prepared NAA solution were added. Both the prepared SA and CMC solutions were mixed and continuously stirred for one hour to obtain a well-dispersed ZnO, NAA and KCl-loaded SA-CMC polymer composite. Next, a saturated $CaCl_2$ solution was prepared. Thereafter, ZnO, NAA, and KCl-loaded SA-CMC polymer composite dispersion was slowly added dropwise to the $CaCl_2$ solution while gently stirring the solution. Here, the bead formation was observed; the beads were then cured in the gelation medium for 15 minutes. Afterwards, the beads were filtered, washed with distilled water and separated. The hydrogel beads were air-dried to evaporate the water and were then stored in a dry container.[60–62] The prepared hydrogels were utilized for the treatment T5, which is mentioned under "2.2.11 Plant assessment".

Hydrogel beads for treatments T2, T3, T4 and T5 were prepared with different combinations of the composition as

Table 1 Different combinations of the compositions of the prepared hydrogel beads

Hydrogel bead formulation for each treatment	Composition of the beads				
	SA (4 w/w%)	CMC (0.8 w/w%)	ZnO NPs (0.4 w/w%)	NAA (0.008 w/w%)	KCl (13.5 w/w%)
T2	√	√		√	
T3	√	√	√		
T4	√	√	√	√	
T5	√	√	√	√	√

tabulated in Table 1, which is discussed later in their application under "2.2.11 Plant assessment".

2.2.4 Characterization of the prepared hydrogel beads. The prepared hydrogel beads were characterized using FTIR analysis and SEM analysis.

2.2.5 Swelling capacity of the hydrogel beads. To study the water-absorbing behavior and swelling capacity of the synthesized hydrogel beads, 1.00 g of dry, SA-CMC polymer-only hydrogel and nutrient-loaded hydrogel were immersed in 50 mL of deionized water and were allowed to swell at room temperature. At the time intervals of 1, 2, 3, 5, 7, 14, and 21 days, swollen beads were removed from the solution using a stainless-steel mesh. The swollen beads were washed with distilled water and excess moisture was removed using filter papers. Both types of hydrogels were weighed, and the swelling capacity was calculated using eqn (1), where W_d was the weight of the dried hydrogel and W_S was the weight of the swollen hydrogel. The results were collected in triplicate in all experiments.[63,64]

$$\text{Swelling capacity}(\%) = \frac{(W_s - W_d)}{W_d} \times 100 \quad (1)$$

2.2.6 Biodegradability test for the hydrogel beads. Biodegradability testing of the prepared hydrogel beads was conducted using the soil burial method, employing the same agricultural soil as in the plant study. One bead of the prepared hydrogel was buried in soil at a depth of approximately 2–3 cm in containers and kept at room temperature under controlled-moisture conditions to overcome water loss *via* evaporation. At the time intervals of 1, 5, 10, 15, and 20 days, beads were unearthed and qualitatively evaluated using visual observation of discoloration, shrinking and disintegration. For this test, the procedure was modified to get observations using an optical microscope. The extent of hydrogel degradation was determined by calculating the weight loss (wt_{loss}) according to eqn (2), where wt_i is the initial weight of the samples before starting the degradation and wt_f is the weight of the sample after specified time intervals of biodegradation. Before reweighing the retrieved hydrogel beads, they were rinsed with distilled water.[36,63,65] The results were collected in triplicate in all experiments.

$$wt_{loss}(\%) = \left[\frac{wt_i - wt_f}{wt_i}\right] \times 100 \quad (2)$$

2.2.7 Quantification of Zn and K nutrient contents in synthesized hydrogel beads. Exactly 104.4 mg of synthesized hydrogel beads were introduced into a beaker containing 2.5 mL of concentrated HNO_3 and 7.5 mL of concentrated HCl. Then, the beaker was heated using a magnetic stirrer until the hydrogel beads were completely dissolved, with the temperature maintained at 90 °C throughout the experiment. The solution obtained was filtered through a 0.45 μm syringe, and the resulting clear solution was analyzed using atomic absorption spectroscopy (AAS) to quantify the amount of Zn and K nutrients in the hydrogel beads by mass.

2.2.8 Release behavior of nutrients in water. Firstly, three hydrogel beads (weighing 51.8 mg) were dipped in a beaker with 25 mL of deionized water at room temperature. The initial pH was recorded upon the addition of beads to deionized water. Aliquots of 1 mL were drawn from the system at intervals of 24 hours and 7, 14, and 21 days by preparing separate systems for each time interval. Each drawn-out aliquot was introduced to a 5 mL volumetric flask and diluted up to the mark. Respective atomic absorbance readings were taken for Zn and K metals separately using atomic absorption spectroscopy. Then, the amount of metal released was calculated using eqn (3), where nut_0 is the initial amount of nutrients in the hydrogel and nut_t is the amount of nutrients released into the water in the time interval t. The collected results were averaged in triplicate in all experiments conducted.[36,64]

$$\text{Nutrient release}(\%) = \frac{(\text{nut}_t)}{\text{nut}_0} \times 100 \quad (3)$$

2.2.9 Encapsulation efficiency of NAA hormone. Encapsulation efficiency (EE) was computed from the total concentration of the prepared NAA solution (c_{total}) and NAA content in dry hydrogel (c_{load}) beads, then EE was calculated using eqn (4), where $c_{load} = c_{total} - c_f$, c_f is the concentration of NAA in the filtrate after separating the hydrogel beads. The NAA concentrations were determined spectrophotometrically.[66]

$$EE(\%) = \left(\frac{c_{load}}{c_{total}}\right) \times 100 \quad (4)$$

2.2.10 NAA hormone release study in water. The synthesized dry hydrogel beads weighing 50.0 mg were dispersed in a beaker containing 50 mL of deionized water at room temperature. The initial pH was recorded upon the addition of beads to water. At time intervals of 5, 20, 25, 45, 90, 120, 180, 210, 300, 330, 450 minutes and 7, 14 and 21 days, the dispersion was stirred, and aliquots were collected. The concentration of NAA was determined by UV-VIS spectrophotometry using

a calibration curve. Results were presented as a percentage of released NAA relative to the total amount of NAA encapsulated in hydrogel beads.[64] All experiments were conducted in triplicate.

2.2.11 Plant assessment. Pot trials for chili (*Capsicum annuum*) were carried out to conduct the plant assessment. Here, 4 different compositions of hydrogel beads were used along with conventional K fertilizer and no fertilizer application. About 3 weeks old chili seedlings, which were grown under equivalent conditions and reached a comparable growth stage, were acquired from a plant nursery and planted in pots, where the potting medium was prepared similarly. For each treatment, 6 seedlings were used, with two seedlings per pot; sunlight, water, and other conditions were provided in a consistent manner to all plants throughout the experiment. Nitrogen and phosphorous sources were provided equally to all plants, excluding the group with no fertilizer application. The synthesized hydrogel beads were applied to the plants after 3 weeks of transplanting the seedlings, as the hydrogel fertilizer is focused on the flowering and fruiting stage of chili. Exactly 1.00 g of hydrogel beads were applied per plant. After the hydrogel beads were applied, observations were taken weekly for 4 weeks for the parameters of plant height (Fig. S4†), while the number of branches, number of flowers, number of pods and the yield at the first plucking at the end of week 4. Plant groups treated with no fertilizer, conventional K fertilizer, hydrogel formulation for T2, hydrogel formulation for T3, hydrogel formulation for T4, and hydrogel formulation for T5 were named as T0, T1, T2, T3, T4, and T5, respectively, for the convenience of identification.

2.2.12 Statistical analysis. Statistical analysis was performed by analysis of variance (ANOVA) and significant difference of each sample was analyzed by Tukey pairwise comparison at the significance level of 0.05.

3. Results and discussion

3.1 Characterization of synthesized zinc oxide nanoparticles

3.1.1 PXRD analysis of synthesized zinc oxide nanoparticles. Crystallographic data of the synthesized ZnO NPs were obtained by the PXRD analysis. The average particle size has been determined from the full width at half maximum (FWHM) of the diffraction peaks using Debye–Scherrer's equation, which is given by $D = K\lambda/\beta \cos \theta$. Here, D is the crystal size in nanometers, K is the Scherrer constant given by 0.9, λ is the X-ray wavelength given by 0.154178 nm, β is the full width of the peak at half maximum in radians, and θ is the XRD peak position in degrees.[59] The PXRD pattern for the synthesized ZnO NPs confirmed the successful synthesis of ZnO NPs, as depicted in Fig. 2.

The PXRD pattern of the synthesized ZnO NPs was obtained in the diffraction angle range $20° \leq 2\theta \leq 80°$. The peaks obtained at 2θ = 31.74°, 34.42°, 36.25°, 47.56°, 56.58°, 62.86°, 66.35°, 67.91°, 69.07°, 72.61°, and 77.01° can be assigned to the (100), (002), (101), (102), (110), (103), (200), (112), (201), (004), and (202) planes, according to JCPDS card number 36-1451, respectively. The peaks obtained matched with the reference PXRD pattern for hexagonal ZnO NPs, confirming that the prepared ZnO NPs are free from impurities (Fig. 2). The absence of additional peaks indicates that the sample contains only one phase of ZnO. The average crystallite size calculated using the Debye–Scherer equation for synthesized ZnO NPs was 39.41 nm (Table S1†).

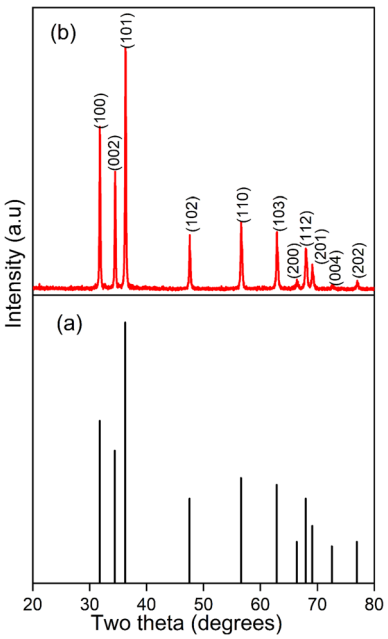

Fig. 2 (a) JCPDS card 36-1451 for ZnO. (b) PXRD spectrum of the synthesized ZnO NPs.

3.1.2 SEM analysis of synthesized zinc oxide nanoparticles. The SEM images of the sample are shown in Fig. 3(A), which reveal that the particles are predominantly spherical-shaped, and rod-shaped nanoparticles are also present. The SEM images are in good agreement with the existing literature.[67] It is observed that particles exhibit a granular nature. Furthermore, agglomeration of particles is observed as primary or secondary agglomeration. Primary agglomeration occurs in the precipitation step, in which high capillary action or high surface tension of $Zn(OH)_2$ particles, which are formulated during the synthesis process of ZnO NPs, agglomerate.[68] Collisions between the particles at the precipitation stage might have caused Smoluchowski ripening, resulting in agglomeration during the precipitation stage. Secondary agglomeration occurs during the drying stage, in which Ostwald ripening can result from the thermal diffusion of nanoparticles to reduce their surface energy.[69] Particle diameter distribution graph in Fig. 3(B) shows that the diameter of the synthesized ZnO NPs lies in the range of 0–300 nm. The average diameter recorded for the synthesized ZnO NPs was 152 nm. A high calcination temperature and low agitation speed might have caused a large particle size.[70]

3.1.3 FTIR analysis of synthesized zinc oxide nanoparticles. The FTIR spectrum in the ESI Fig. S1† exhibits a broad absorption peak at 3442 cm^{-1} for the stretching mode of vibration of hydroxyl compounds.[71] The peak at 1631 cm^{-1} is assigned to the bending vibrational mode of O–H in H_2O molecules.[71] The band at 439 cm^{-1} corresponds to the metal–oxygen (Zn–O stretching vibrations) vibration mode, which lies

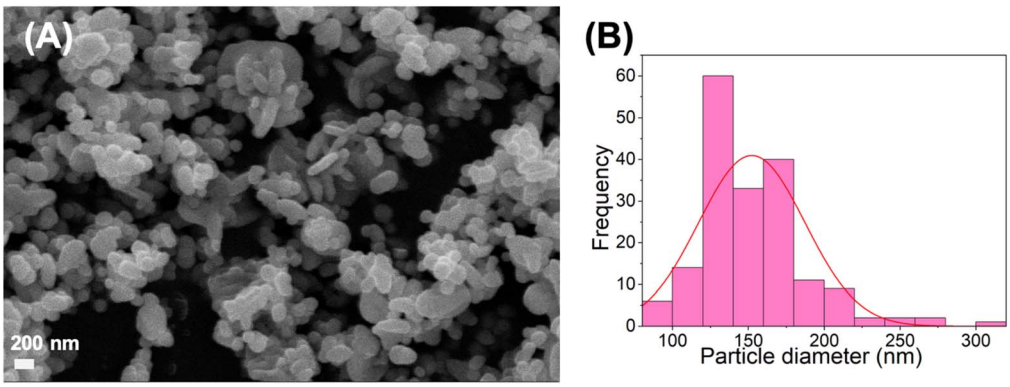

Fig. 3 (A) SEM image of ZnO NPs at a scale bar of 200 nm and a magnification of 25 000×. (B) Particle diameter distribution of the synthesized ZnO NPs.

within the fingerprint region.[72] The peak at 1384 cm^{-1} is attributed to the symmetric C=O vibration of atmospheric CO_2.[73] The peak at 1114 cm^{-1} is attributed to the C–O stretching. The peak at 2340 cm^{-1} is for the asymmetric C=O vibration of atmospheric CO_2.[74]

3.2 Characterization of synthesized hydrogel beads

3.2.1 SEM analysis of synthesized hydrogel beads. The synthesized hydrogel beads are shown in Fig. 4. SEM analysis was done to determine the morphological features of the synthesized hydrogel beads. SEM images in Fig. 5 show the microporous structure of the hydrogel beads. They confirm the presence of polymers along with ZnO NPs. The surface appears to have an irregular pattern owing to the complex structural composition of the beads. Cavities are visible on the surface alongside the cracks, which might have occurred during the drying process of the beads. A higher number of cavities allows the fertilizer solution to be entrapped into micro-environmental cavities and diffused into the hydrogel bead easily due to the capillary effect. The distribution of the ZnO NPs on the surface was observed in a random manner, although the distribution was not dense. This could be attributed to NPS either participating in cross-linking or being embedded within the beads. However, the presence of ZnO NPs was confirmed in the hydrogel beads, which was further verified *via* elemental composition analysis data provided from energy-dispersive X-ray spectroscopy (EDX) (Fig. S2†).

Fig. 4 Synthesized hydrogel beads.

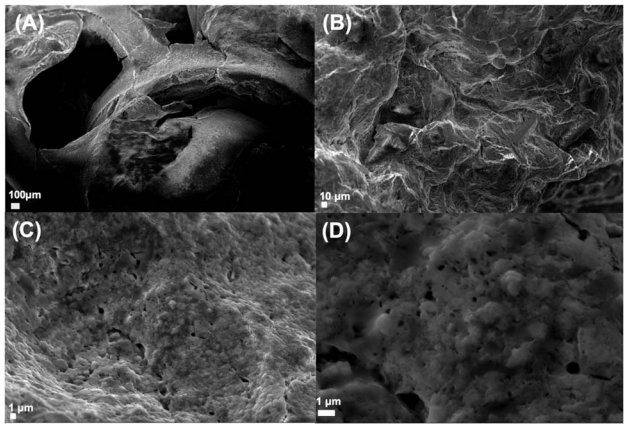

Fig. 5 SEM images of the synthesized hydrogel beads; with scale bars and magnifications at (A) 100 μm, 75 000× (B) 10 μm, 500 000× (C) 1 μm, 5000× and (D) 1 μm, 15 000×

3.2.2 FTIR analysis of synthesized hydrogel beads. The FTIR spectra of SA (Fig. 6) show an intense characteristic peak at 3446 cm^{-1}, which corresponds to the stretching mode of vibration of O–H in H_2O molecules, while the band observed at 2930 cm^{-1} could be attributed to the asymmetric $-CH_2$ stretching vibrations. The bands observed at 1634 and 1415 cm^{-1} were attributed to the stretching of carboxylate anions and the C–OH deformation with a contribution from the O–C–O symmetric stretching of carboxylate groups, respectively. A less intense band at 1106 cm^{-1} can be attributed to the C–O stretching vibrations of the pyranose rings. The band observed at 929 cm^{-1} could be attributed to the C–O stretching of uronic acid residues.[75]

The FTIR spectra of CMC (Fig. 6) show an intense characteristic peak at 3455 cm^{-1}, which corresponds to the stretching mode of vibration of O–H in H_2O molecules, while the band observed at 2925 cm^{-1} can be assigned to the asymmetric $-CH_2$ stretching vibrations.[75] At 1745 cm^{-1}, there is a sharp absorption band, which indicates the stretching vibration of the carboxyl compound (COO^-), while the peak at 1454 cm^{-1}

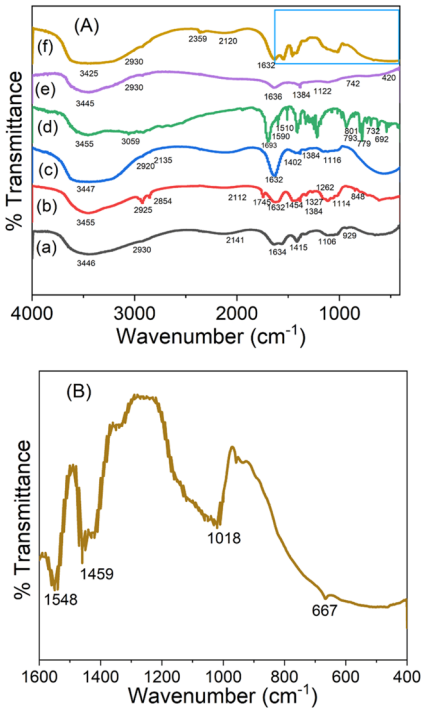

Fig. 6 (A) FTIR spectra of (a) SA, (b) CMC; (c) Ca^{2+} crosslinked SA-CMC, (d) NAA; (e) SA-CMC loaded with ZnO NPs; and NAA (f) SA-CMC loaded with ZnO NPs, NAA, and KCl. (B) FTIR spectrum of hydrogel beads in the range 1600–400 cm^{-1}.

corresponds to the stretching vibration of the carboxyl compound in the form of salt. The peak at 1384 cm^{-1} can be attributed to the symmetrical deformation of the CH_2 group.[77] The peak at 1327 cm^{-1} can be attributed to the asymmetric C–O stretching.[76] The peaks at 1262 and 1114 cm^{-1} could be attributed to the C–O–C stretching vibration of the ether group.[77]

The FTIR spectrum of the Ca^{+2}-crosslinked SA-CMC hydrogel (Fig. 6) exhibits the peaks at 1384 and 1402 cm^{-1}, which can be attributed to the COO^- symmetric stretching vibrations. The peak at 1632 cm^{-1} can be attributed to the COO^- asymmetric stretching vibrations. A broad absorption peak at 3447 cm^{-1} can be attributed to the stretching mode of vibration of O–H in H_2O molecules. The peak at 1116 cm^{-1} can be attributed to the C–O–C stretching. The peak at 2135 cm^{-1} can be attributed to the CO_2 vibration. The peak at 2920 cm^{-1} can be attributed to the asymmetric CH_2 stretching.[78]

The FTIR spectrum of NAA (Fig. 6) shows a broad peak at 3455 cm^{-1}, which corresponds to the –OH stretching in the H_2O molecule. The peak at 3059 cm^{-1} was assigned to aromatic C–H stretching, a characteristic region allowing ready identification of the structure. The peak at 1693 cm^{-1} could be an overtone and combination band that occurred due to the C–H out-of-plane deformation vibrations. Sharp peaks at 1510 and 1590 cm^{-1} correspond to the C=C stretching vibrations of the aromatic ring structure. Peaks at 692 732, 779, 793, and 801 cm^{-1} correspond to the C–H in-plane bending vibrations of the aromatic ring.[79]

The FTIR spectrum for the hydrogel of SA-CMC loaded with ZnO NPs and NAA hormone (Fig. 6) shows a peak at 3445 cm^{-1}, which corresponds to the –OH stretching in H_2O molecules. The peak observed at 2930 cm^{-1} can be attributed to asymmetric CH_2 stretching, while the peak at 1636 cm^{-1} can be attributed to –COO asymmetric stretching vibrations, resulting from the dissociation of the carboxylic acid groups in sodium alginate, CMC and NAA hormone. The peak at 1384 cm^{-1} indicates the symmetric bending vibrations of –COO groups.[78] The peak at 1122 cm^{-1} could be attributed to the C–O–C stretching vibrations, while the peak at 742 cm^{-1} can be attributed to the ring-in-plane vibrations in aromatic compounds, likely corresponding to the aromatic structure of naphthalene acetic acid, indicating its presence in the hydrogel bead.[78,79] The peak at 420 cm^{-1} could be assigned to the metal oxygen vibrations, indicating the stretching mode of Zn–O.[72]

The FTIR spectrum of the SA-CMC loaded with ZnO NPs, NAA and KCl (Fig. 6) depicted a broad peak at 3425 cm^{-1}, corresponding to the –OH stretching vibrations.[78] The peak at 2930 cm^{-1} can be assigned to the asymmetric CH_2 stretching, while the peak at 2359 cm^{-1} indicates the presence of CO_2, which can occur as a byproduct of the reactions that occurred. The peak observed at 1632 cm^{-1} can be attributed to the –COO asymmetric stretching vibrations from carboxylic acid or carboxylate groups present in SA, CMC and NAA.[77] The peak at 1459 cm^{-1} can be associated with the symmetric bending vibrations of –COOH, indicating the presence of ionized carboxylic acid groups, whereas the peak at 1018 cm^{-1} is likely related to C–O–C stretching vibrations, which can arise from ether or alcohol functionalities from sodium alginate and CMC.[77,78] The peak at 667 cm^{-1} was attributed to the metal oxygen vibrations, indicating the stretching mode of Zn–O.[72] However, a characteristic peak for KCl is not observed in the spectrum, which could be due to its ionic nature. The overlapping nature of some peaks due to the complex interactions between and among the components of the hydrogel bead could be reflected in the absence of a sharp, characteristic peak attributed to KCl which can be verified by other means of characterizations, such as SEM-EDX, which confirmed the elemental composition, detecting K in the sample.

3.3 Study of the swelling capacity of the synthesized hydrogel beads

The swelling capacity of the hydrogel was compared with that of the hydrogel synthesized only with SA and CMC polymers crosslinked with $CaCl_2$. As illustrated in Fig. 7, the swelling capacity of both hydrogels increased with time and reached an equilibrium swelling capacity, which was maintained until the end of the experimentation period. The SA-CMC polymer-only hydrogel attained its equilibrium swelling capacity on day 7 with a 31.25%, while the hydrogel reached its maximum on day 14 with a reported swelling capacity of 202.04% with a slight decrement observed on day 21 (195.01%); otherwise, a stable state of swelling capacity was observed until the end of the experimentation period.

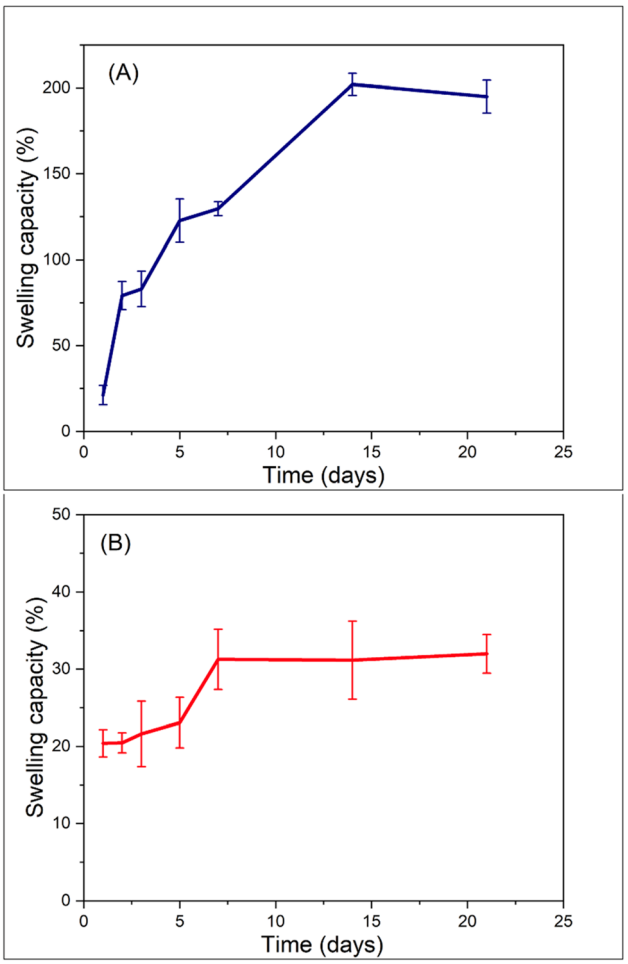

Fig. 7 Swelling capacity of the (A) hydrogel and (B) SA-CMC beads.

Swelling capacity is mainly determined by the structure of the hydrogel, polymerization process, concentration of the cross-linking agent and particle size of the hydrogel, with the concentration of the cross-linking agent having the most impact.[80] SA and CMC are polymers rich in carboxylic groups, making them hydrophilic and enabling the absorption of large amounts of water and swelling. Upon crosslinking, Ca^{2+} ions bind to the carboxylate groups in SA and CMC *via* strong ionic interactions, forming a 3D network. Studies show swelling inversely relates to the crosslinker concentration; at higher cross-linking, pore spaces are reduced as the number of cross-links in the polymer chain increases. The swelling capacity of SA-CMC beads is significantly lower than that of hydrogel beads, which is consistent with the observation that pure SA-CMC beads exhibit higher cross-linking, resulting in limited porosity. A homogeneous Ca^{2+} cross-linking reduces the surface area for water penetration, whereas hydrogel beads exhibit an increased swelling capacity, which increases approximately to 202.04% after 14 days.[81]

The higher swelling behavior of hydrogel beads can also be attributed to the incorporation of ZnO NPs into the beads, as they introduce nanopores and surface roughness, increasing water diffusion pathways.[82]

Furthermore, K^+ ions from KCl encapsulated in the polymer matrix of the hydrogel beads have a lower charge density than Ca^{2+}, forming weaker ionic bonds that allow greater chain flexibility and swelling. Literature states that monovalent cations having a lower charge with a large ionic radius impart a positive influence, resulting in maximum swelling; in contrast, cations with a bivalent charge and small ionic size impart a comparatively negative influence, resulting in less swelling.[80] The cations exhibit swelling in the following order: $K^+ > Na^+ > Ca^{2+} > Mg^{2+}$.[83] Since both Ca^{2+} ions and K^+ ions are present in the hydrogel beads, competitive ion exchange between K^+ and Ca^{2+} reduces the effective crosslinking density. The resulting crosslinked network is less rigid than that of SA-CMC beads with greater chain flexibility. Limited swelling (31.25%) of SA-CMC beads cross-linked with $CaCl_2$ could be attributed to their dense network and lack of additional porosity, enhancing components in contrast to the hydrogel beads.

3.4 Biodegradability test for the synthesized hydrogel beads

As depicted in Fig. 8, the hydrogel beads exhibited an increasing degradation with significant weight loss over time, as such 12.26% after 24 hours, accounting for the initial swelling and erosion of the beads, while 53.16% after 5 days, indicating the breakdown of the polymer network, 85.46% at the end of day 10, illustrating a substantial matrix disintegration and 95.01% after 15 days, nearing complete degradation while 99.98% at the end of day 20, indicating almost total bead disintegration. This rapid and near-complete degradation within 20 days suggests that the hydrogel matrix is biodegradable, satisfying the objective of ensuring biodegradability in the synthesized hydrogel beads.

In Fig. 9, the optical microscopy images further confirmed the degradation process. Initially, on day 0, the beads appeared with smooth and undamaged surfaces, and on days 5 and 10, the beads showed shrinkage and irregularities consistent with

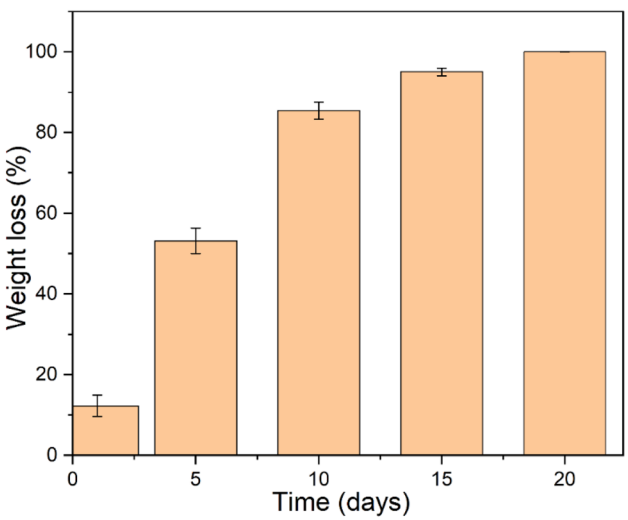

Fig. 8 Weight loss percentages of hydrogel beads for the period of 20 days.

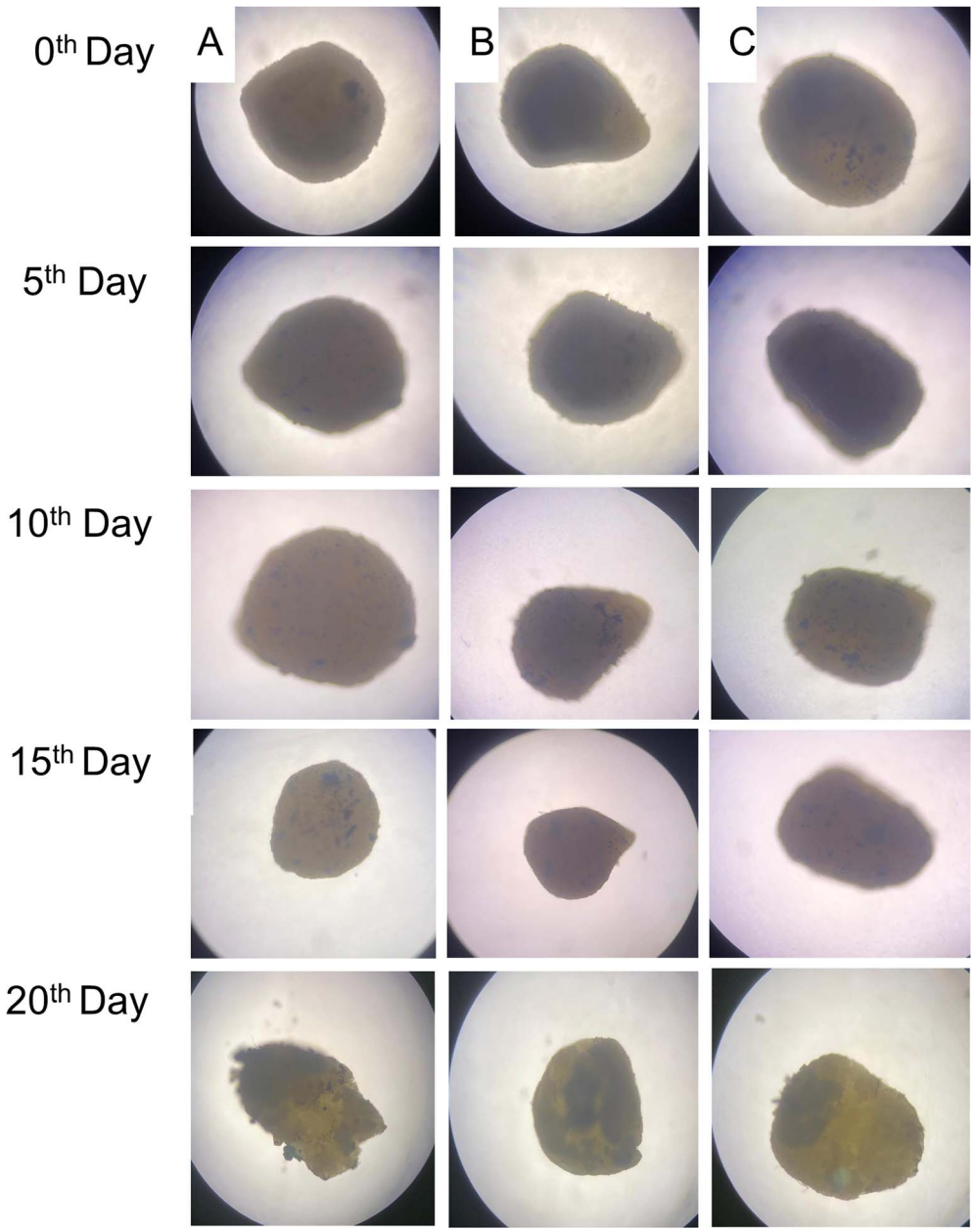

Fig. 9 Optical microscopy images (40×) of three replicate hydrogel beads (A–C) taken from the same sample during the 20-day soil-burial test ($n = 3$).

weight loss and swelling of the beads. By day 15, the beads were substantially reduced in size and even exhibited fragmentation. By day 20, shapes were visible with irregularities and almost complete disintegration, confirming the weight loss data. Increased brittleness was observed in the beads over time, as they were buried under soil for a longer period, resulting in chipping at the edges of the beads, which became visible by day 20.

These observations are consistent with the reported studies, where Passauer *et al.* confirmed that after 14 days, significant biodegradation was observed in a quantitative biodegradation test done for lignin-based hydrogel using biomineralization.[84] Additionally, Gabriel *et al.* demonstrated that by day 18, discoloration and shriveling of the hydrogel were observed in the soil biodegradability test done for sodium-CMC/SA/hydroxypropyl cellulose hydrogel film.[63]

Swelling capacity and biodegradation rate are said to have a complementary relationship, as degradation commences with the occurrence of hydrolysis, which is continued by the activity of microorganisms. Additionally, the porous structures of hydrogels allow for the leakage of water and microorganisms, facilitating the successful degradation of hydrogels.[85] In this study, swelling capacity and degradation were computed as 202.04% and 95.01%, respectively (by day 14 and day 15), which is consistent with the earlier reported finding. This observation was further supported by the fact that the growth cycle of chili

was completed after 28 days of fertilizer application. Essentially, the first plucking was done on day 28, thus encapsulated nutrients were effectively released while beads were biodegraded.

3.5 Quantification of Zn and K contents of the synthesized hydrogel beads

Upon analyzing the results of AAS, it was quantified that in a hydrogel sample of 104.40 mg, nutrients K and Zn were present in a total mass of 14.96 ± 0.13 mg and 1.82 ± 0.00 mg, accounting for a total nutrient % content of 14.33% and 1.74%, respectively.

The AAS results showed the successful loading of ZnO NPs and KCl into the synthesized hydrogel beads. The loaded K content is much higher than that of Zn, as a macronutrient, an increased presence of K is needed compared to the micronutrient Zn. However, the weight% of Zn is relatively low, which could be increased to ensure that the content does not exceed the critical Zn level to be non-toxic to the plant.

3.6 Release of nutrients in water at pH 7.2

The K release profile in Fig. 10(A) exhibited fluctuations over the 21-day period, with release percentages of 9.79% in 24 hours, decreasing to 5.48% in 7 days, then increasing to 16.19% in 14

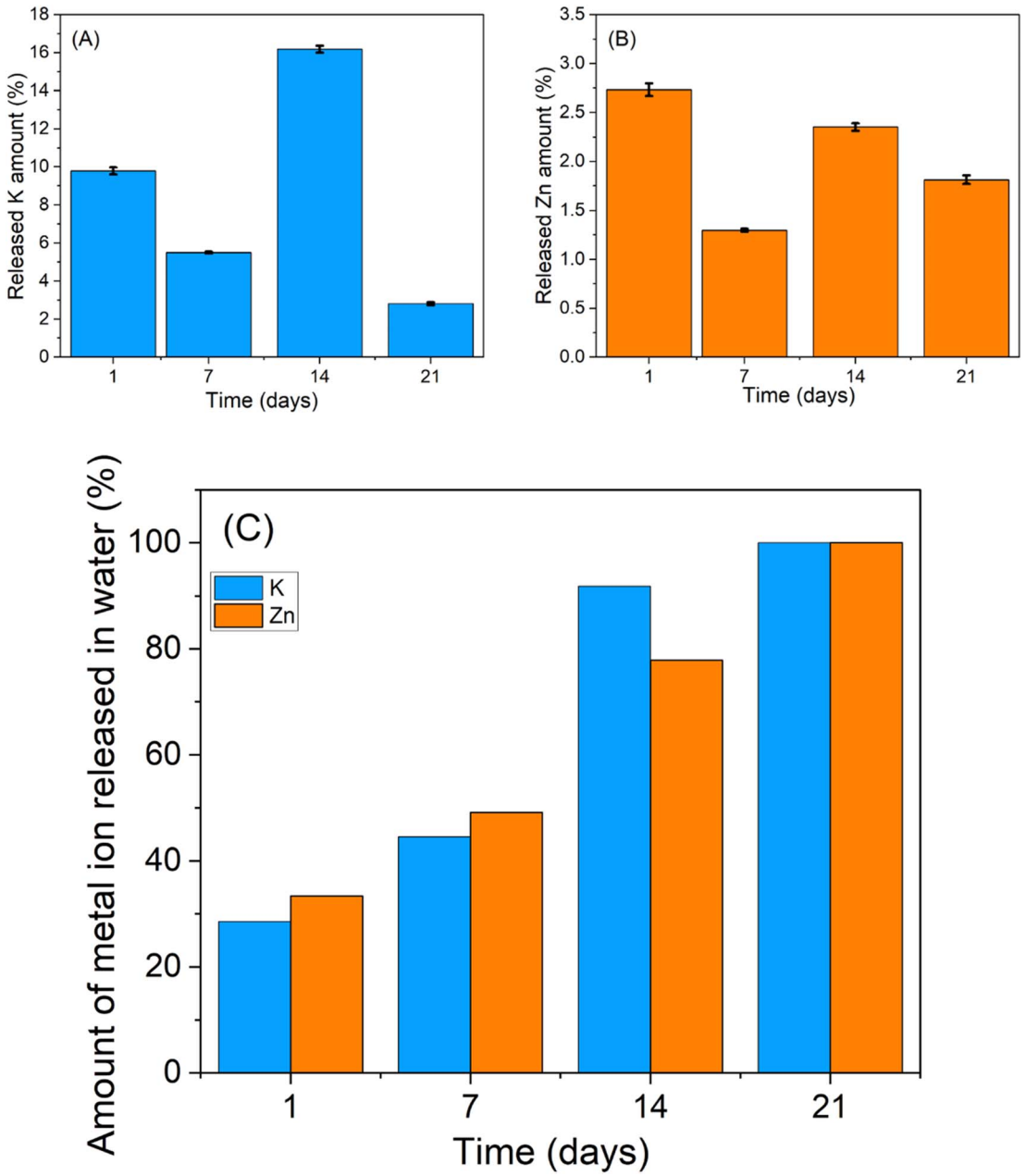

Fig. 10 Pattern of the release of the hydrogel in water showing the variation of (A) K ion% and (B) Zn ion% in water in a period of 21 days, and (C) cumulative percentage release of the nutrients with time in water, compared with the total amount released within the experimentation period.

days, followed by a decline to 2.81% in 21 days. In matrix-type hydrogels, such as the synthesized hydrogel in this study, nutrient release is governed by various mechanisms, such as diffusion, swelling or degradation in the polymer. At instances where diffusion alone is the driving factor for the release of encapsulated nutrients, the concentration gradient between the medium and the polymer network causes water molecules to diffuse through the hydrogel network, carrying and facilitating nutrient transport. In contrast, fluctuations observed in the release profiles support the fact that release is not solely governed by the concentration gradient, suggesting that this behavior is consistent with the characteristics observed in the non-Fickian (anomalous) diffusion, where the release mechanism involves a collective effort of polymer chain relaxation and diffusion.[86] However, the mechanism followed in release behavior should be further investigated by fitting the data to a semi-empirical kinetic model, like the Korsmeyer–Peppas model.[87]

The zinc release in Fig. 10(B) from the synthesized hydrogel showed low cumulative percentages at the measured intervals: 2.73% at 24 hours, decreasing to 1.30% at 7 days, increasing again to 2.35% at 14 days, and then decreasing slightly to 1.81% at 21 days. This overall low and fluctuating release profile indicates a very slow and controlled zinc diffusion from the hydrogel matrix. The SA-CMC hydrogel crosslinked with Ca^{2+} forms a dense, highly crosslinked network hindering the mobility and immediate release of zinc ions from ZnO NPs to the surrounding medium. Additionally, the initial burst release could be attributed to the fact that ZnO NPs, held in the SA-CMC matrix by weak interactions, are released initially to the medium, followed by a decrease in release on day 7. Again, on day 14, an increase is observed, followed by a slight decline on day 21. This observation can be explained by the fact that the hydrogel undergoes swelling over time, which by day 14 shows a swelling capacity exceeding 200% (202.04%); hence, ZnO NPs in the deeper layers of the hydrogel beads are released into the medium. Moreover, slight re-adsorption occurrences might have caused the zinc ions to temporarily re-associate with the hydrogel matrix, resulting in these fluctuations. Similar observations were reported in the release study of zinc and copper metals from an alginate-based hydrogel nanofertilizer.[88]

Swelling is a characteristic feature of hydrogels, which plays a pivotal role in nutrient release. When hydrogels are added to water, they absorb water, eventually turning into a swollen gel. Initially, the fertilizers in the outer layer of the hydrogel are readily dissolved in water, resulting in an increase in nutrient content in the release medium, which is consistent with the observations for the K and Zn release in this study. A concentration gradient for fertilizers occurred at this instance, causing them to be released to the water medium. However, the complex internal morphology and porous structure in the polymer matrix may hinder this sustained release, which could be attributed to the fluctuations observed for the nutrient release profiles in this study.[86]

Upon understanding the swelling dynamics of the synthesized hydrogel, the increased swelling capacity on days 7 and 14 at 129.72% and 202.04%, respectively, indicates that the hydrogel swelled more between days 7 and 14, thereby increasing the diffusion of K and explaining the higher release on day 14. Conversely, reduced swelling by day 21 might have caused a slight decrease in K release. Similarly, the release profile of Zn was 1.30%, 2.35%, and 1.81% on days 7, 14 and 21, respectively, which can be attributed to the swelling dynamics observed. Additionally, Ghobashy *et al.* reported similar release profiles for nitrogen and phosphorous from a multifunctional poly(vinyl pyrrolidone)-based superabsorbent hydrogel, where occasional decreases in release profile were observed.[89]

Fig. 10(C) shows the percentage release of nutrients in water with time, compared to the total amount of these metals released in water within the experimental period. These observations reveal that more than 40% of the total released nutrient content, which was released throughout the experimentation period, occurred within the first 14 days. The increased release could be attributed to the fact that nutrients in deeper layers were released into the water as swelling occurred simultaneously; by day 21, almost complete release was observed as the crosslinked network gradually degraded, allowing the remaining nutrients to diffuse out. This observation is in good agreement with the degradability study, which showed that by day 20, 99.98% of the hydrogel was degraded.

However, both nutrients showed an initial burst release, followed by a sustained phase with slight fluctuations, fulfilling the objective of a slow-release fertilizer for agricultural applications. Moreover, the swelling-controlled release mechanisms have improved nutrient availability, paving the way for efficient and sustainable fertilizer applications.

3.7 Encapsulation efficiency of NAA hormone

Encapsulation efficiency of the NAA hormone in hydrogel beads is 92.53%, which is a considerably higher value. This could be attributed to the compact structure formed by the SA-CMC matrix upon crosslinking with saturated $CaCl_2$. Ionic crosslinking between alginate and Ca^{2+} forms an "egg-box" structure, effectively entrapping the NAA hormone and preventing leakage.[37] Higher encapsulation efficiency can also be assigned to the mechanical strength gained by encapsulating nanoparticles. As reported by Mandal *et al.*, the incorporation of nanoparticles positively affects the characteristics of the polymer network, optimizing water retention and mechanical strength, eventually allowing the nutrients and agrochemicals encapsulated within the matrix to be released in a sustained manner.[86]

3.8 Release of NAA hormone in water

The release of NAA showed a gradual increase (Fig. 11(A)), which peaked at 450 minutes, with 58.12% of NAA being released. The first half of the graph illustrates this "initial burst release", which provides an initial dose of NAA to the plants after application. This behavior can be explained by the fact that a considerable amount of NAA is adsorbed onto the outer surface or loosely bound to the outer layers of the hydrogel beads.[90] In the second half, a sustained release is observed with slight fluctuations until day 14. From day 1 to day 14, the almost

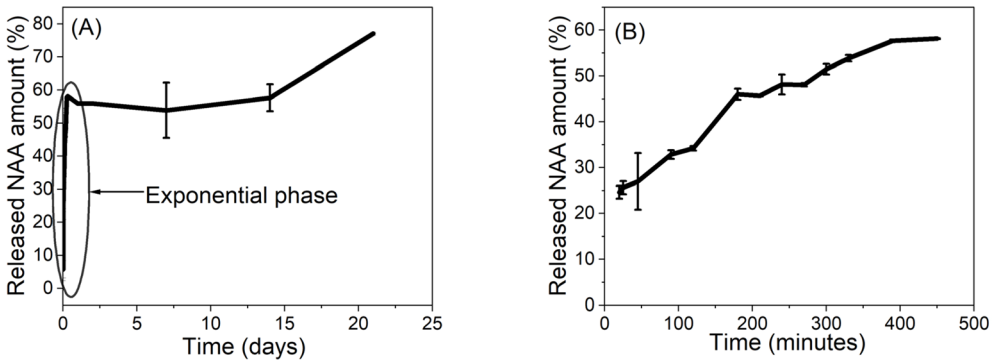

Fig. 11 (A) Released NAA% with time from the hydrogel beads for a period of 21 days. (B) Exponential phase of NAA release profile for 20–450 minutes.

stationary phase visible could be due to the release attaining a temporary equilibrium, where the rate of NAA diffusion matches its availability within the matrix. However, the fluctuations observed could be due to the hormone either degrading or an amount of the hormone being re-adsorbed into the polymer matrix with the increased concentration of hormone in water. It is possible that components of the hydrogel, apart from NAA, which will also be released with time, could have acted as chelating agents, destroying the original structure of NAA. Additionally, other released components could be forming complexes with released NAA, which results in decreased detection of the released NAA within this time.

Observations from days 1 to 14 ensure the steady and slow-release behavior of the hormone, further optimizing the formulation of hydrogel beads to achieve either a higher total release or more prolonged release duration of NAA. However, within 4 weeks after applying the hydrogel, the first plucking of chili harvest was obtained, supporting the suitability of this hydrogel.

The phase during which the exponential behavior of NAA was observed from 20–450 minutes was fitted into different kinetic models. According to Table S2,† the R^2 values obtained by fitting the exponential phase to the zeroth order, first order, Korsmeyer–Peppas and Higuchi models (Fig. S3†) suggested that the first half of the NAA release fits best with the Higuchi model, as it has the highest value for R^2 (0.97). This indicates that diffusion is the primary mechanism governing NAA release during this phase, and the cumulative amount of nutrient released was proportional to the square root of time, reflecting a diffusion-controlled process based on Fick's law.[13] The NAA release accelerated during this exponential phase, as illustrated in Fig. 11(B), which might be due to the increased diffusion of NAA from the deeper layers of the hydrogel matrix. This model further assumes a uniform initial concentration of the nutrient, constant diffusivity, and a perfect sink condition where the released nutrient is immediately removed from the release site.[13,91]

However, in a study carried out by Vlahoviček-Kahlina *et al.*, where chitosan/alginate microcapsules were loaded with novel synthesized PGRs, their release profiles were illustrated, exhibiting a rapid initial PGR release, followed by a slower release with its kinetics according to the Korsmeyer–Peppas model.[66] Additionally, another study, which used slow-released NPK fertilizer encapsulated by NaAlg-*g*-poly(AA-*co*-AAm)/MMT superabsorbent nanocomposites, showed that the release of fertilizers followed the Fickian diffusion mechanism, and the release data in both water and soil fitted well with Higuchi and Korsmeyer–Peppas models.[92]

This dual-phase release makes the synthesized hydrogel an effective fertilizer for agricultural use, ensuring both immediate and an extended period of availability of plant hormones. It is observed on day 21 that there is a significant increase in release, which could be due to the degradation of the hydrogel, reported as 99.98% by day 20, which could have caused the deeply embedded hormone molecules to leave the polymer matrix. This degradation could cause the matrix to have expanded pores in the beads, increasing the diffusion rate of the hormone. However, by the end of day 21, 76.99% of NAA has been released, which signifies that incorporating the NAA hormone into the hydrogel bead is effective as a slow-release fertilizer. The remaining percentage of NAA, which has not been released, could be due to some NAA being tightly bound within the matrix region or present in more tightly crosslinked areas, making NAA difficult to release. By day 20, the hydrogel is almost completely degraded, implying that after day 20, the remaining NAA entrapped within should be released.

3.9 Statistical analysis of the plant assessment

A statistical analysis was performed by analysis of variance (ANOVA), and the significant difference of each sample was analyzed by Tukey pairwise comparison at a significance level of 0.05. Tables S3 and S4† present the mean value ± SD ($n = 6$) with Tukey's HSD letter annotations for the observed parameters, while Fig. S5 and S6† graphically represent the statistical difference between treatments along with the Tukey HSD letter annotations.

3.9.1 Study of the effect of hydrogel beads on the height of plants. The ANOVA test results confirmed that T5 had a significant effect on plant height over time. Week 0 showed no significant difference among all treatments as expected, due to the fertilizers not being applied in week 0. In week 1, T5 was

significantly taller than T0, while the other treatments showed no significant differences from either treatment group. From weeks 2–4, T5 consistently recorded the highest heights, significantly exceeding T0 and sometimes T1 and T2, T1-T4 were generally grouped as "ab–bc", indicating intermediate performance.

The pronounced height increases in T5 relative to T2 and T0 suggest that the plants in the T5 group uptake nutrients more effectively, supporting the evidence of improved NUE with encapsulated components. It is understood that T5 significantly enhanced plant height from week 1 onwards, while other formulations led to moderate but not consistently superior growth.

3.9.2 Study of the effect of hydrogel beads on the number of branches of plants. T5 has shown the highest branching count, significantly greater than T0 and T1. Treatments T2–T4 are intermediate, not significantly different from T5. The synergistic effect of the formulation could be attributed to this observation, positioning T5 as an effective treatment compared to all other treatments.

3.9.3 Study of the effect of hydrogel beads on the number of flowers of plants. The plant group treated with T5 has significantly outperformed T0, while the T1–T4 treatments have clustered in the "ab" group, overlapping with both, indicating no significant difference from either.

3.9.4 Study of the effect of hydrogel beads on the number of pods of plants. The number of pods was the highest in T5, followed by T2, T3 and T4, which were not significantly different from each other and T1 and T0, which had significantly fewer pods.

3.9.5 Study of the effect of hydrogel beads on the yield of plants. The plant group treated with T5 had the highest yield, which was significantly greater than that of T0 and T1. Yields for T2, T3, and T4 are not significantly different from each other but are higher than that of T0.

The results clearly demonstrate that the T5 treatment (hydrogel formulation of SA-CMC-NAA-ZnO NPs-KCl) leads to significantly improved plant performance across the measured parameters-branching, flowering, pod formation, and yield-compared to both the control (T0) and conventional K fertilizer (T1). The consistent superiority of T5, as shown by its unique statistical grouping, highlights the efficacy of this multifunctional formulation. The intermediate performance of T2, T3, and T4 suggests that each component contributes to improved plant performance, but the addition of KCl in T5 provides an additive or synergistic effect, maximizing the benefits. This aligns with the fact that integrating nanotechnology, plant growth regulators and targeted nutrient delivery can enhance plant development beyond what is achievable with traditional fertilizers alone.

It is observed that the boosted performance of T5 likely stems from improved NUE. The economic value of plants like chili is mainly dependent on the crop yield; hence, improved yield and a probable higher NUE from the T5 hydrogel formulation are promising for sustainable agriculture by improving crop productivity and potentially minimizing the environmental impact caused by traditional fertilizers alone. It is imperative to direct future studies focusing on long-term field trials, economic feasibility and agronomic benefits of synthesized formulations like T5.

4. Conclusion

In the pursuit of sustainable agricultural practices, this study demonstrated that synthesizing a biopolymer-based integrated hydrogel formulation holds significant value for improving crop yield in short-term crops, such as chili, as well as diminishing the negative consequences caused by traditional fertilizers. ZnO NPs, KCl and NAA hormone were successfully encapsulated into the synthesized hydrogel matrix, where their swelling capacity, biodegradability and the release profiles of nutrients and hormone were studied. The synthesis of ZnO NPs was performed through a surfactant-assisted, co-precipitation method, and the characterization was done *via* XRD, SEM and FTIR analyses. The synthesized hydrogel was characterized *via* FTIR and SEM analysis, where the presence of ZnO was confirmed by FTIR and the presence of Zn was confirmed by SEM-EDX analyses. The presence of K and NAA was confirmed by AAS and UV-vis spectrophotometry, respectively. The encapsulation of NAA along with ZnO NPs and KCl showcased the potential of the synthesized hydrogel formulation as a plant protection product rather than a traditional fertilizer. The biodegradability study verified the eco-friendliness of the synthesized hydrogel, positioning it as a sustainable option. The swelling capacity study demonstrated that the hydrogel showed a remarkable increase in swelling compared to the SA-CMC polymer-only hydrogel bead, implying that the encapsulation improved the water-absorbing capacity of the hydrogels.

The release profiles verified a slow-release pattern of the said nutrients and hormone. The synthesized hydrogels were applied to chili plants, focusing on their flowering and fruiting stages; the results of statistical analysis suggested that the height, number of branches, flowers, pods and yield had increased mean values in the plant group treated with the integrated hydrogel formulation. Statistical significance was observed in the number of flowers between the hydrogel-treated plant group (T5) and all other treatments. A significant difference in yield value was observed in the hydrogel formulation (T5)-treated plant group compared to other treatments, indicating its potential as a sustainable alternative to obtain an increased fruit yield. Furthermore, it was noted that the polymeric network complex could be further developed for multifunctional hydrogel formulations, which can provide nutrients and hormones in a sustained manner for other growth stages as well as for improved agricultural productivity.

Data availability

All the data are included in the manuscript.

Author contributions

Loshini Rodrigo – formal analysis, investigation, and writing – original draft, Imalka Munaweera – conceptualization,

methodology, resources, supervision, and writing-review and editing, Pamoda Thavish Perera-conceptualization, methodology, resources, supervision, and writing-review and editing.

Conflicts of interest

The authors declare no conflict of interest.

Acknowledgements

The authors thank the Department of Chemistry in the University of Sri Jayewardenepura and Research and Development Division of Panam Biotech (Pvt) Ltd, Homagama for providing the necessary facilities to conduct this research study, the Instrument Center in the Faculty of Applied Sciences in the University of Sri Jayewardenepura for their support with the relevant instrumental operation and analyses. The authors also thank Ms Piumika Yapa for the support provided in obtaining the optical microscopy images related to this manuscript.

References

1 United Nations, *Global Issues: Population*, United Nations, New York, **https://www.un.org/en/global-issues/population**.
2 Z. Li and M. Zhang, Progress in the preparation of stimulus-responsive cellulose hydrogels and their application in slow-release fertilizers, *Polymers*, 2023, **15**(17), 3643, DOI: **10.3390/polym15173643**.
3 Food and Agriculture Organization of the United Nations, *Transforming Food and Agriculture to Achieve the SDGs*, FAO, Rome, **https://www.fao.org/family-farming/detail/en/c/1145621/**.
4 Intergovernmental Panel on Climate Change. *Special Report on Climate Change and Land*, IPCC, Geneva, **https://www.ipcc.ch/srccl/**.
5 Z. Tariq, D. N. Iqbal, M. Rizwan, M. Ahmad, M. Faheem and M. Ahmed, Significance of biopolymer-based hydrogels and their applications in agriculture: a review in perspective of synthesis and their degree of swelling for water holding, *RSC Adv.*, 2023, **13**(35), 24731–24754, DOI: **10.1039/d3ra03472k**.
6 K. Ali, Z. Asad, H. D. A. Gamareldawla, A. Saud, A. Khan and S. J. Zaidi, Progress and innovations in hydrogels for sustainable agriculture, *Agronomy*, 2024, **14**(12), 2815, DOI: **10.3390/agronomy14122815**.
7 G. N. Nguyen and N. Lantzke, Mitigating the adverse effects of semi-arid climate on *Capsicum* cultivation by using the retractable roof production system, *Plants*, 2022, **11**(20), 2794, DOI: **10.3390/plants11202794**.
8 C. A. Damalas and I. G. Eleftherohorinos, Pesticide exposure, safety issues, and risk assessment indicators, *Int. J. Environ. Res. Public Health*, 2011, **8**(5), 1402–1419, DOI: **10.3390/ijerph8051402**.
9 S. Govil, V. Duc, M. Escribà-Gelonch and V. Hessel, Controlled-release fertiliser: recent developments and perspectives, *Ind. Crops Prod.*, 2024, **219**, 119160, DOI: **10.1016/j.indcrop.2024.119160**.
10 S. Yang, L. Wang, K. Akhtar, I. Ahmad and A. Khan, Optimizing nitrogen fertilization and variety for millet grain yield and biomass accumulation in dry regions, *Agronomy*, 2022, **12**(9), 2116, DOI: **10.3390/agronomy12092116**.
11 H. Shaghaleh, Y. Alhaj Hamoud, X. Xu, S. Wang and H. Liu, A pH-responsive/sustained release nitrogen fertilizer hydrogel based on aminated cellulose nanofiber/cationic copolymer for application in irrigated neutral soils, *J. Clean. Prod.*, 2022, **368**, 133098, DOI: **10.1016/j.jclepro.2022.133098**.
12 M. H. Hossain, M. A. K. Azad, E. B. Soren, M. N. Alam, M. S. Ahmed, M. S. Islam, *et al.*, Enhancing growth, yield, and nutritional value of Capsicum annuum: evaluating micronutrient efficiency and varietal performance, *J. Agric. Food Res.*, 2025, **21**, 101945, DOI: **10.1016/j.jafr.2025.101945**.
13 N. Lakshani, H. Wijerathne, C. Sandaruwan, N. Kottegoda and V. Karunarathne, Release kinetic models and release mechanisms of controlled-release and slow-release fertilizers, *ACS Agric. Sci. Technol.*, 2023, **3**(11), 939–956, DOI: **10.1021/acsagscitech.3c00152**.
14 T. Jamja, S. F. Akhtar and R. Tabing, Controlled release fertilizers and their coating with natural polymers, *Agric. Food: e-Newslett.*, 2024, **6**, 410–412.
15 P. L. Kashyap, X. Xiang and P. Heiden, Chitosan nanoparticle based delivery systems for sustainable agriculture, *Int. J. Biol. Macromol.*, 2015, **77**, 36–51, DOI: **10.1016/j.ijbiomac.2015.02.039**.
16 E. Ye and X. J. Loh, Polymeric hydrogels and nanoparticles: a merging and emerging field, *Aust. J. Chem.*, 2013, **66**(9), 997, DOI: **10.1071/ch13168**.
17 J. G. Lyons, L. M. Geever, M. J. D. Nugent, J. E. Kennedy and C. L. Higginbotham, Development and characterisation of an agar–polyvinyl alcohol blend hydrogel, *J. Mech. Behav. Biomed. Mater.*, 2009, **2**(5), 485–493, DOI: **10.1016/j.jmbbm.2008.12.003**.
18 D. Merino and A. A. Vera, Advanced applications of green materials in agriculture, in *Applications of Advanced Green Materials*, Woodhead Publishing, 2021, pp. 193–222, DOI: **10.1016/b978-0-12-820484-9.00008-8**.
19 M. O. Rahman, M. A. Halim, A. Deb, S. Ahmed, M. W. Rahman, N. C. Dafader, *et al.*, Modification of superabsorbent hydrogels for industrial wastewater treatment, *Adv. Polym. Technol.*, 2022, **2022**, 1–10, DOI: **10.1155/2022/8405230**.
20 R. Liang, H. Yuan, G. Xi and Q. Zhou, Synthesis of wheat straw-g-poly(acrylic acid) superabsorbent composites and release of urea from it, *Carbohydr. Polym.*, 2009, **77**(2), 181–187, DOI: **10.1016/j.carbpol.2008.12.018**.
21 N. Saruchi, B. S. Kaith, R. Jindal and G. S. Kapur, Synthesis of gum tragacanth and acrylic acid based hydrogel: its evaluation for controlled release of antiulcerative drug pantoprazole sodium, *J. Chin. Adv. Mater. Soc.*, 2014, **2**(2), 110–117, DOI: **10.1080/22243682.2014.911114**.
22 A. I. Raafat, M. Eid and M. B. El-Arnaouty, Radiation synthesis of superabsorbent CMC based hydrogels for agriculture applications, *Nucl. Instrum. Methods Phys. Res., Sect. B*, 2012, **283**, 71–76, DOI: **10.1016/j.nimb.2012.04.011**.

23 H. A. A. El-Rehim, E.-S. A. Hegazy and H. L. A. El-Mohdy, Preparation and characterization of poly(acrylamide-co-acrylate) hydrogels for controlled release applications, *J. Appl. Polym. Sci.*, 2004, **93**, 1360–1371.

24 R. A. Ramli, Slow release fertilizer hydrogels: a review, *Polym. Chem.*, 2019, **10**(45), 6073–6090, DOI: 10.1039/c9py01036j.

25 C. Bai, S. Zhang, L. Huang, H. Wang, W. Wang and Q. Ye, Starch-based hydrogel loading with carbendazim for controlled-release and water absorption, *Carbohydr. Polym.*, 2015, **125**, 376–383, DOI: 10.1016/j.carbpol.2015.03.004.

26 A. El Idrissi, F. Tayi, O. Dardari, Y. Essamlali, I. Jioui, I. Ayouch, *et al.*, Urea-rich sodium alginate-based hydrogel fertilizer as a water reservoir and slow-release N carrier for tomato cultivation under different water-deficit levels, *Int. J. Biol. Macromol.*, 2024, **272**, 132814, DOI: 10.1016/j.ijbiomac.2024.132814.

27 A. K. Rana, V. K. Gupta, P. R. Hart and V. K. Thakur, Cellulose-alginate hydrogels and their nanocomposites for water remediation and biomedical applications, *Environ. Res.*, 2024, **243**, 117889, DOI: 10.1016/j.envres.2023.117889.

28 M. Shahriari-Khalaji, S. Hong, G. Hu, Y. Ji and F. F. Hong, Bacterial nanocellulose-enhanced alginate double-network hydrogels cross-linked with six metal cations for antibacterial wound dressing, *Polymers*, 2020, **12**(11), 2683, DOI: 10.3390/polym12112683.

29 H. Xie, H. Xia, L. Huang, Z. Zhong, Q. Ye, L. Zhang and A. Lu, Biocompatible, antibacterial and anti-inflammatory zinc ion cross-linked quaternized cellulose-sodium alginate composite sponges for accelerated wound healing, *Int. J. Biol. Macromol.*, 2021, **191**, 27–39, DOI: 10.1016/j.ijbiomac.2021.09.047.

30 K. I. Draget, O. Smidsrød and G. Skjåk-Bræk, Alginates from algae, in *Biopolymers Online*, ed. A. Steinbüchel, Wiley-VCH, Weinheim, 2005, DOI: 10.1002/3527600035.bpol6008.

31 H. Grasdalen, B. Larsen and O. Smidsrød, A P.m.r. study of the composition and sequence of uronate residues in alginates, *Carbohydr. Res.*, 1979, **68**(1), 23–31, DOI: 10.1016/s0008-6215(00)84051-3.

32 H. J. Kong, K. Y. Lee and D. J. Mooney, Decoupling the dependence of rheological/mechanical properties of hydrogels from solids concentration, *Polymer*, 2002, **43**(23), 6239–6246, DOI: 10.1016/s0032-3861(02)00559-1.

33 G. T. Grant, E. R. Morris, D. A. Rees, P. J. C. Smith and D. Thom, Biological interactions between polysaccharides and divalent cations: the egg-box model, *FEBS Lett.*, 1973, **32**(1), 195–198, DOI: 10.1016/0014-5793(73)80770-7.

34 B. Beig, M. B. K. Niazi, F. Sher, Z. Jahan, U. S. Malik, M. D. Khan, *et al.*, Nanotechnology-based controlled release of sustainable fertilizers. A review, *Environ. Chem. Lett.*, 2022, **20**, 2709–2726, DOI: 10.1007/s10311-022-01409-w.

35 A. Olad, H. Zebhi, D. Salari, A. Mirmohseni and A. R. Tabar, Water retention and slow release studies of a salep-based hydrogel nanocomposite reinforced with montmorillonite clay, *New J. Chem.*, 2018, **42**(4), 2758–2766, DOI: 10.1039/c7nj03667a.

36 E. G. Arafa, M. W. Sabaa, R. R. Mohamed, A. M. Elzanaty and O. F. Abdel-Gawad, Preparation of biodegradable sodium alginate/carboxymethylchitosan hydrogels for the slow-release of urea fertilizer and their antimicrobial activity, *React. Funct. Polym.*, 2022, **174**, 105243, DOI: 10.1016/j.reactfunctpolym.2022.105243.

37 R. Liu and R. Lal, Potentials of engineered nanoparticles as fertilizers for increasing agronomic productions, *Sci. Total Environ.*, 2015, **514**, 131–139, DOI: 10.1016/j.scitotenv.2015.01.104.

38 A. Singh, N. B. Singh, S. Afzal, T. Singh and I. Hussain, Zinc oxide nanoparticles: a review of their biological synthesis, antimicrobial activity, uptake, translocation and biotransformation in plants, *J. Mater. Sci.*, 2017, **53**(1), 185–201, DOI: 10.1007/s10853-017-1544-1.

39 C. Noulas, M. Tziouvalekas and T. Karyotis, Zinc in soils, water and food crops, *J. Trace Elem. Med. Biol.*, 2018, **49**, 252–260, DOI: 10.1016/j.jtemb.2018.02.009.

40 M. Faizan, J. A. Bhat, C. Chen, M. N. Alyemeni, L. Wijaya, P. Ahmad and F. Yu, Zinc oxide nanoparticles (ZnO-NPs) induce salt tolerance by improving the antioxidant system and photosynthetic machinery in tomato, *J. Trace Elem. Med. Biol.*, 2021, **161**, 122–130, DOI: 10.1016/j.plaphy.2021.02.002.

41 X. Q. Zhou, Z. Hayat, D. D. Zhang, M. Y. Li, S. Hu, Q. Wu, *et al.*, Zinc oxide nanoparticles: synthesis, characterization, modification, and applications in food and agriculture, *Processes*, 2023, **11**, 1193, DOI: 10.3390/pr11041193.

42 R. Raliya, R. Nair, S. Chavalmane, W. N. Wang and P. Biswas, Mechanistic evaluation of translocation and physiological impact of titanium dioxide and zinc oxide nanoparticles on the tomato (Solanum lycopersicum L.) plant, *Metallomics*, 2015, **7**(12), 1584–1594, DOI: 10.1039/C5MT00168D.

43 C. O. Dimkpa, J. Andrews, J. Fugice, U. Singh, P. S. Bindraban, W. H. Elmer, J. L. Gardea-Torresdey and J. C. White, Facile Coating of Urea With Low-Dose ZnO Nanoparticles Promotes Wheat Performance and Enhances Zn Uptake Under Drought Stress, *Front. Plant Sci.*, 2020, **11**, 168, DOI: 10.3389/fpls.2020.00168.

44 K. Mi, X. Yuan, Q. Wang, C. Dun, R. Wang, S. Yang, Y. Yang, H. Zhang and H. Zhang, Zinc oxide nanoparticles enhanced rice yield, quality, and zinc content of edible grain fraction synergistically, *Front. Plant Sci.*, 2023, **14**, 1196201, DOI: 10.3389/fpls.2023.1196201.

45 F. Zahra, F. A. Utami, G. C. S. Girsang, S. Z. S. M. Mulya, V. D. Fentiana, Y. K. Putri and A. B. D. Nandiyanto, Economic evaluation of zinc oxide nanoparticle production through green synthesis method using *Cassia fistula* plant extract, *Int J Educ Couns.*, 2024, **5**(2), 18–24, DOI: 10.47238/ijeca.v5i2.133.

46 J. L. Soto-Gonzales, J. V. González-Fernández, D. D. Pinzón-Moreno, E. C. Vicuña-Galindo and M. V. Carranza-Oropeza, Influence of hydrogel and zinc oxide nanoparticles on the germination and establishment of *Chenopodium quinoa*, *Life*, 2024, **14**(9), 1163, DOI: 10.3390/life14091163.

47 Y. Uysal, Z. G. Doğaroğlu, Z. Çaylali and D. S. Karakulak, Rosemary-mediated green synthesis of ZnO nanoparticles and their integration into hydrogel matrices: evaluating effects on wheat growth and antibacterial properties, *Glob. Chall.*, 2024, **8**(11), 2400120, DOI: 10.1002/gch2.202400120.

48 M. Radmehr, A. Poursattar Marjani and A. Akhavan, Synthesis and characterization of antibacterial CMC/AAc/ZnO nanocomposite superabsorbent using gamma radiation, *Sci. Rep.*, 2025, **15**, 9345, DOI: 10.1038/s41598-025-93884-8.

49 K. Kakar, N. A. Wahocho, N. U. N. Memon, G. M. Jamro, M. N. Kandhro, M. Anwar and Naqeebullah, Assessing the effect of potassium nutrition on the chilies (Capsicum annuum L.) nursery growth and production, *J Appl Res Plant Sci.*, 2024, **5**(2), 183–189, DOI: 10.38211/joarps.2024.05.235.

50 M. Akram, S. Hussain, A. Hamid, S. Majeed, S. A. Chaudary, Z. A. Shah, *et al.*, Interactive effect of phosphorus and potassium on growth, yield, quality and seed production of chili (Capsicum annuum L.), *J. Hortic.*, 2017, **4**(1), 192, DOI: 10.4172/2376-0354.1000192.

51 N. L. Slameto, I. Fariroh, R. Y. Rusdiana and K. Hariyono, Effects of potassium fertilizer on growth, capsaicin, and ascorbic acid content of local and hybrid chili (Capsicum annum L.), *Plant Cell Biotechnol. Mol. Biol.*, 2021, 337–345.

52 Y. S. Chen, S. W. Phang, A. S. Shuib and J. L. Tee, Release behavior and biodegradability of controlled-release potassium fertilizer encapsulated in starch–alginate matrix, *Asia-Pac. J. Chem. Eng.*, 2023, **18**(6), e2998, DOI: 10.1002/apj.2998.

53 A. E. L. Sabagh, S. Mbarki, A. Hossain, M. A. Iqbal, M. S. Islam, A. Raza, A. Llanes, M. Reginato, M. A. Rahman, W. Mahboob, R. K. Singhal, A. Kumari, K. Rajendran, A. Wasaya, T. Javed, R. Shabbir, J. Rahim, C. Barutçular, U. R. Habib, M. A. Raza, D. Ratnasekera, Ö. Konuskan, M. A. Hossain, V. S. Meena, S. Ahmed, Z. Ahmad, M. Mubeen, K. Singh, M. Skalicky, M. Brestic, O. Sytar, E. Karademir, C. Karademir, M. Erman and M. Farooq, Potential Role of Plant Growth Regulators in Administering Crucial Processes Against Abiotic Stresses, *Front. Agron.*, 2021, **3**, 648694, DOI: 10.3389/fagro.2021.648694.

54 Y. L. Sun and S. K. Hong, Effects of plant growth regulators and L-glutamic acid on shoot organogenesis in the halophyte Leymus chinensis (Trin.), *Plant Cell Tissue Organ Cult.*, 2009, **100**(3), 317–328, DOI: 10.1007/s11240-009-9653-4.

55 S. K. Singh, A. Kumar, K. Beer, V. P. Singh and S. K. Patel, Effect of naphthalene acetic acid (NAA) and gibberellic acid (GA3) on growth and fruit quality of tomato (Lycopersicon esculentum Mill.), *Int. J. Curr. Microbiol. Appl. Sci.*, 2018, **7**(03), 306–311, DOI: 10.20546/ijcmas.2018.703.036.

56 A. R. Khan, W. Azhar, X. Fan, Z. Ulhassan, A. Salam, M. Ashraf, Y. Liu and Y. Gan, Efficacy of zinc-based nanoparticles in alleviating the abiotic stress in plants: current knowledge and future perspectives, *Environ. Sci. Pollut. Res. Int.*, 2023, **30**(51), 110047–110068, DOI: 10.1007/s11356-023-29993-6.

57 S. M. Khardia, Y. K. Ghilotia, L. P. Balai and I. B. Sethi, Effect of plant growth regulators and zinc fertilization on growth of pearlmillet (Pennisetum glaucum (L.) R. Br. emend Stuntz), *Int. J. Curr. Microbiol. Appl. Sci.*, 2020, **9**(12), 3161–3168, DOI: 10.20546/ijcmas.2020.912.376.

58 A. U. Jan, A. Shah and F. Hadi, Role of potassium, zinc and gibberellic acid in increasing drought stress tolerance in sunflower (helianthus annuus l.), *Pakistan J. Bot.*, 2019, **51**(3), 809–815, DOI: 10.30848/PJB2019-3(4).

59 A. C. Mohan and B. Renjanadevi, Preparation of zinc oxide nanoparticles and its characterization using scanning electron microscopy (SEM) and X-ray diffraction (XRD), *Procedia Technol.*, 2016, **24**, 761–766, DOI: 10.1016/j.protcy.2016.05.078.

60 S. M. Ibrahim, F. I. Abou El Fadl and A. A. El-Naggar, Preparation and characterization of crosslinked alginate–CMC beads for controlled release of nitrate salt, *J. Radioanal. Nucl. Chem.*, 2013, **299**(3), 1531–1537, DOI: 10.1007/s10967-013-2820-4.

61 S. K. Bajpai and S. Sharma, Investigation of swelling/degradation behaviour of alginate beads crosslinked with Ca^{2+} and Ba^{2+} ions, *React. Funct. Polym.*, 2004, **59**(2), 129–140, DOI: 10.1016/j.reactfunctpolym.2004.01.002.

62 T. Jamnongkan and S. Kaewpirom, Potassium release kinetics and water retention of controlled-release fertilizers based on chitosan hydrogels, *J. Polym. Environ.*, 2010, **18**(3), 413–421, DOI: 10.1007/s10924-010-0228-6.

63 R. G. Garduque, B. J. Gococo, C. A. Yu, P. J. Nalzaro and T. Tumolva, Synthesis and characterization of sodium carboxymethyl cellulose/sodium alginate/hydroxypropyl cellulose hydrogel for agricultural water storage and controlled nutrient release, *Solid State Phenom.*, 2020, **304**, 51–57, DOI: 10.4028/www.scientific.net/ssp.304.51.

64 K. F. Hendrawan, Y. Sonjaya and N. Chotimah, Physical and chemical characteristics of alginate-poly(vinyl alcohol) based controlled release hydrogel, *J. Environ. Chem. Eng.*, 2016, **4**(4), 4863–4869, DOI: 10.1016/j.jece.2016.03.043.

65 R. Saberi Riseh, M. Gholizadeh Vazvani, M. Hassanisaadi and Y. A. Skorik, Micro-/nano-carboxymethyl cellulose as a promising biopolymer with prospects in the agriculture sector: a review, *Polymers*, 2023, **15**(2), 440, DOI: 10.3390/polym15020440.

66 K. Vlahoviček-Kahlina, S. Jurić, M. Marijan, *et al.*, Synthesis, characterization, and encapsulation of novel plant growth regulators (PGRs) in biopolymer matrices, *Int. J. Mol. Sci.*, 2021, **22**(4), 1847, DOI: 10.3390/ijms22041847.

67 M. Deylami, E. Alizadeh, M. Sarikhani, M. Hejazy and M. Firouzamandi, Zinc oxide nanoparticles promote the aging process in a size-dependent manner, *J. Mater. Sci. Mater. Med.*, 2021, **32**(10), 128, DOI: 10.1007/s10856-021-06602-x.

68 B. Wang, W. Zhang, W. Zhang, *et al.*, Influence of drying processes on agglomeration and grain diameters of magnesium oxide nanoparticles, *Dry. Technol.*, 2007, **25**(4), 715–721, DOI: 10.1080/07373930701291108.

69 D. K. Pattadar and F. P. Zamborini, Effect of size, coverage, and dispersity on the potential-controlled Ostwald ripening of metal nanoparticles, *Langmuir*, 2019, **35**(50), 16416–16426, DOI: 10.1021/acs.langmuir.9b02421.

70 D. B. Lade and A. S. Shanware, hytonanofabrication: methodology and factors affecting biosynthesis of nanoparticles, in *Smart Nanosystems for Biomedicine, Optoelectronics and Catalysis*, 2020, DOI: 10.5772/intechopen.90918.

71 R. Wahab, S. G. Ansari, M. A. Dar, Y. S. Kim and H. S. Shin, Synthesis of magnesium oxide nanoparticles by sol-gel process, *Mater. Sci. Forum*, 2007, **559**, 983–986, DOI: 10.4028/www.scientific.net/msf.558-559.983.

72 C. Amutha, S. Thanikaikarasan, V. Ramadas, S. A. Bahadur, B. Natarajan and R. Kalyani, Synthesis, characterization and antibacterial efficiency of ZnO nanoparticles using rice as soft bio-template, *Optik*, 2016, **127**(10), 4281–4286, DOI: 10.1016/j.ijleo.2016.01.124.

73 M. Vafaee and M. S. Ghamsari, Preparation and characterization of ZnO nanoparticles by a novel sol–gel route, *Mater. Lett.*, 2007, **61**(15), 3265–3268, DOI: 10.1016/j.matlet.2006.11.089.

74 S. Jurablu, M. Farahmandjou and T. Firoozabadi, Sol-gel synthesis of zinc oxide (ZnO) nanoparticles: study of structural and optical properties, *J. Sci. Islam. Repub. Iran*, 2015, **26**(3), 281–285.

75 F. Araiza-Verduzco, E. Rodríguez-Velázquez, H. Cruz, *et al.*, Photocrosslinked alginate-methacrylate hydrogels with modulable mechanical properties: effect of the molecular conformation and electron density of the methacrylate reactive group, *Materials*, 2020, **13**(3), 534, DOI: 10.3390/ma13030534.

76 S. Hidayat, P. Ardiaksa, N. Riveli and I. Rahayu, Synthesis and characterization of carboxymethyl cellulose (CMC) from salak-fruit seeds as anode binder for lithium-ion battery, *J. Phys.:Conf. Ser.*, 2018, **1080**, 012017, DOI: 10.1088/1742-6596/1080/1/012017.

77 K. Mikula, D. Skrzypczak, B. Ligas and A. Witek-Krowiak, Preparation of hydrogel composites using Ca^{2+} and Cu^{2+} ions as crosslinking agents, *SN Appl. Sci.*, 2019, **1**(6), 643, DOI: 10.1007/s42452-019-0657-3.

78 S. Ramadhani and H. Helmiyati, Alginate/CMC/ZnO nanocomposite for photocatalytic degradation of Congo red dye, *AIP Conf. Proc.*, 2020, **2242**, 040026, DOI: 10.1063/5.0008095.

79 V. Krishnakumar, R. Mathammal and S. Muthunatesan, FT-IR and Raman spectra vibrational assignments and density functional calculations of 1-naphthyl acetic acid, *Spectrochim. Acta, Part A*, 2008, **70**(1), 210–216, DOI: 10.1016/j.saa.2007.06.040.

80 M. Rizwan, S. R. Gilani, A. I. Durani and S. Naseem, Materials diversity of hydrogel: synthesis, polymerization process and soil conditioning properties in agricultural field, *J. Adv. Res.*, 2021, **33**, 15–40, DOI: 10.1016/j.jare.2021.03.007.

81 N. F. C. Nan, N. Zainuddin and M. Ahmad, Preparation and swelling study of CMC hydrogel as potential superabsorbent, *Pertanika J Sci Technol*, 2019, **27**(1), 489–498.

82 B. Kumar, R. Priyadarshi, Sauraj, *et al.*, Nanoporous sodium carboxymethyl cellulose-g-poly(sodium acrylate)/FeCl3 hydrogel beads: synthesis and characterization, *Gels*, 2020, **6**(4), 49, DOI: 10.3390/gels6040049.

83 Y. Bao, J. Ma and N. Li, Synthesis and swelling behaviors of sodium carboxymethyl cellulose-g-poly(AA-co-AM-co-AMPS)/MMT superabsorbent hydrogel, *Carbohydr. Polym.*, 2011, **84**(1), 76–82, DOI: 10.1016/j.carbpol.2010.10.061.

84 L. Passauer, T. Hallas, E. Bäucker, G. Ciesielski, S. Lebioda and U. Hamer, Biodegradation of hydrogels from oxyethylated lignins in model soils, *ACS Sustain. Chem. Eng.*, 2015, **3**(9), 1955–1964, DOI: 10.1021/acssuschemeng.5b00139.

85 G. Dalei, S. Das, S. R. Jena, *et al.*, Improved chemosensitization activity of carboxymethyl chitosan/PVA hydrogels by plasma surface modification, *J. Polym. Environ.*, 2021, **29**(5), 1663–1679, DOI: 10.1007/s10924-020-02007-z.

86 M. Mandal, R. S. Lodhi, S. Chourasia, S. Das and P. Das, A review on sustainable slow-release N, P, K fertilizer hydrogels for smart agriculture, *ChemPlusChem*, 2025, **90**(3), e202400643, DOI: 10.1002/cplu.202400643.

87 M. Włodarczyk, H. Siwek, K. Lubkowski and A. Buchwał, Release of selected nutrients from polymer-coated fertilisers in the soil environment, *J. Water Land Dev.*, 2024, 201–211, DOI: 10.24425/jwld.2024.151568.

88 S. A. Ekanayake and P. I. Godakumbura, Synthesis of a dual-functional nanofertilizer by embedding ZnO and CuO nanoparticles on an alginate-based hydrogel, *ACS Omega*, 2021, **6**(40), 26262–26272, DOI: 10.1021/acsomega.1c03271.

89 M. M. Ghobashy, M. A. Amin, A. E. Mustafa, *et al.*, Synthesis and application of a multifunctional poly(vinyl pyrrolidone)-based superabsorbent hydrogel for controlled fertilizer release and enhanced water retention in drought-stressed Pisum sativum plants, *Sci. Rep.*, 2024, **14**(1), 27734, DOI: 10.1038/s41598-024-76255-7.

90 M. Li, M. A. Tshabalala and G. Buschle-Diller, Formulation and characterization of polysaccharide beads for controlled release of plant growth regulators, *J. Mater. Sci.*, 2016, **51**(9), 4609–4617, DOI: 10.1007/s10853-016-9775-0.

91 M. P. Paarakh, P. A. Jose, C. Setty and G. Peter Christoper, Release kinetics – concepts and applications, *Int. J. Pharm. Res. Technol.*, 2023, **8**(1), 12–20, DOI: 10.31838/ijprt/08.01.02.

92 A. Rashidzadeh and A. Olad, Slow-released NPK fertilizer encapsulated by NaAlg-*g*-poly(AA-*co*-AAm)/MMT superabsorbent nanocomposite, *Carbohydr. Polym.*, 2014, **114**, 269–278, DOI: 10.1016/j.carbpol.2014.08.010.